Molecular Cell
Article

Collaborative Dynamic DNA Scanning by Nucleotide Excision Repair Proteins Investigated by Single-Molecule Imaging of Quantum-Dot-Labeled Proteins

Neil M. Kad,[1,*] Hong Wang,[2,3] Guy G. Kennedy,[4] David M. Warshaw,[4] and Bennett Van Houten[2,3,*]
[1]Department of Biological Sciences, University of Essex, Colchester, Essex CO4 3SQ, UK
[2]Department of Pharmacology and Chemical Biology, University of Pittsburgh School of Medicine
[3]The University of Pittsburgh Cancer Institute, Hillman Cancer Center
University of Pittsburgh, Pittsburgh, PA 15213, USA
[4]Department of Molecular Physiology & Biophysics, University of Vermont, Burlington, VT 05405, USA
*Correspondence: nkad@essex.ac.uk (N.M.K.), vanhoutenb@upmc.edu (B.V.H.)
DOI 10.1016/j.molcel.2010.02.003

SUMMARY

How DNA repair proteins sort through a genome for damage is one of the fundamental unanswered questions in this field. To address this problem, we uniquely labeled bacterial UvrA and UvrB with differently colored quantum dots and visualized how they interacted with DNA individually or together using oblique-angle fluorescence microscopy. UvrA was observed to utilize a three-dimensional search mechanism, binding transiently to the DNA for short periods (7 s). UvrA also was observed jumping from one DNA molecule to another over ~1 μm distances. Two UvrBs can bind to a UvrA dimer and collapse the search dimensionality of UvrA from three to one dimension by inducing a substantial number of UvrAB complexes to slide along the DNA. Three types of sliding motion were characterized: random diffusion, paused motion, and directed motion. This UvrB-induced change in mode of searching permits more rapid and efficient scanning of the genome for damage.

INTRODUCTION

One of the fundamental questions in the field of DNA repair is how a modest number of repair proteins scan through several million (for bacteria) to a few billion (for mammalian cells) base pairs of nondamaged DNA to find rare damaged bases. How proteins locate their cognate recognition sequences has been extensively studied over the years (von Hippel and Berg, 1986, 1989), and several modes of searching have been hypothesized and recently reviewed (Gorman and Greene, 2008). It is generally believed that facilitated diffusion in a one-dimensional (1D) search greatly enhances the rate of site location. However, direct sliding along DNA could be hampered by the numerous proteins bound to DNA inside a living cell. Thus, other searching modes such as hopping or intersegmental transfer have been proposed.

Nucleotide excision repair (NER) is a generalized DNA repair system capable of recognizing and removing a diverse array of chemical and physical DNA lesions, such as UV-induced photoproducts and carcinogen-DNA adducts (Batty and Wood, 2000; Friedberg et al., 1995, 2006; Sancar, 1996). This highly conserved process is mediated by the concerted action of several proteins. NER is initiated by DNA distortion detection and then followed by: (1) damage verification, (2) coordinated incisions, (3) excision of an oligonucleotide containing the damaged base, (4) repair synthesis, and (5) ligation. In humans, a deficiency in any one of the 7 out of the ~30 NER proteins required for efficient repair can lead to the syndrome xeroderma pigmentosum, characterized by high incidence of skin cancer and, in some cases, neurodegeneration (Lehmann, 2001; Takayama et al., 1996).

UvrA and UvrB are the proteins that mediate damage recognition during NER (Goosen and Moolenaar, 2001; Sancar and Rupp, 1983; Truglio et al., 2006a; Van Houten et al., 2005). Approximately 20–50 copies of UvrA and UvrB are normally found per *E. coli* cell; however, SOS response induction mediated by LexA results in a further 5- to 10-fold induction of the UvrA and UvrB proteins (Sancar and Sancar, 1988). The crystal structures and function analysis of UvrA (Pakotiprapha et al., 2008), UvrB (Machius et al., 1999; Nakagawa et al., 1999; Sohi et al., 2000; Theis et al., 1999; Truglio et al., 2006b; Waters et al., 2006), and UvrC (Karakas et al., 2007; Truglio et al., 2005) have helped delineate the molecular interactions and action mechanism of each protein during the coordinated damage recognition and repair process.

UvrA as a dimer interacts with UvrB to form either a $UvrA_2B$ or $UvrA_2B_2$ complex (Orren and Sancar, 1990; Verhoeven et al., 2002; Wang et al., 2006); for simplicity, we refer to these complexes as UvrAB hereafter. During damage recognition UvrA is hypothesized to recognize helical distortions induced in the DNA rather than the actual modified nucleotide (DellaVecchia et al., 2004; Van Houten et al., 2005). UvrA initiates damage verification through derepression of an autoinhibitory domain (domain 4) (Wang et al., 2006) on UvrB (Truglio et al., 2006b). UvrB engages the damaged site through a β-hairpin, causing dissociation of UvrA (Truglio et al., 2006b). UvrC then binds, producing dual incisions surrounding the damage (Truglio

et al., 2006a; Van Houten et al., 2005). In the final steps of NER, DNA polymerase I and UvrD (helicase II) remove the postincision complex and synthesize the repair patch, which is sealed by DNA ligase (Caron et al., 1985; Husain et al., 1985). Despite the structural and biochemical information available about these proteins, the dynamics of these interactions on DNA remain elusive. To help elucidate this problem, we have turned to single-molecule approaches (Wang et al., 2006, 2008), which have previously been successfully employed for the study of other DNA protein systems, including EcoRV diffusion on DNA (Bonnet et al., 2008); Rad51 involved in recombination (Granéli et al., 2006); hOgg1, a glycosylase involved in base excision repair (Blainey et al., 2006); and the action of mismatch repair heterodimer of Msh2-Msh6 (Gorman et al., 2007).

In this present study, we have created a robust visualization platform for protein-DNA interactions at the single-molecule level. Specifically, using highly fluorescent quantum dots (Qdots) to label individual UvrA and UvrB molecules, we observed the interactions and molecular movements of these proteins on λ-DNA "tightropes." Based on this approach, we report here that damage recognition during NER involves an initial 3D search by UvrA, which collapses into a 1D search when UvrB is added. Unexpectedly, we have found that UvrAB has a complex motion on DNA and appears to display unbiased diffusion, directed motion, and paused motion. Finally, differential labeling of both UvrA and UvrB with different color Qdots has uniquely allowed direct visualization of a protein complex of two separate protein partners loading onto DNA and dissociating during the process of NER.

RESULTS

To achieve single-molecule resolution of repair protein interactions with DNA, we developed a holistic approach to overcome the three key imaging limitations: (1) fluorescence signal intensity and prevention of fluorophore photobleaching, (2) isolation of the DNA from the surface, and (3) reduction of background signals. This was achieved in three stages. First, we labeled our proteins with Qdot nanocrystals (Figure 1A), which possess high quantum yields, can be excited by a continuum of wavelengths, and are highly resistant to photobleaching. Second, we raised the DNA above the surface using a "DNA tightrope" assay (Figure 2A). This permitted the DNA to be visualized extended rather than in its usual collapsed form (Movie S1). Furthermore, potential interactions with the surface that would alter protein migration on the DNA could be eliminated. Such artifacts may be present with techniques that directly apply the DNA to a surface. Third, the architecture of the DNA platform necessitated the application of a unique illumination strategy to reduce background fluorescence.

Qdot Conjugation and UvrA/UvrB Activity

To observe proteins interacting with the DNA tightropes, we conjugated Qdots to UvrA and UvrB proteins (see Supplemental Information). We have previously reported on a Qdot conjugation strategy for UvrB. A nine-residue HA tag was added to UvrB's N terminus, which was subsequently conjugated to the Qdot via an antibody sandwich (Wang et al., 2008) (Figure 1A). In order to avoid cross-reactivity, we used a second strategy to conjugate Qdots to UvrA. BirA biotin ligase was used to attach biotin, with greater than 90% efficiency (data not shown), to a C-terminally engineered biotin ligase recognition sequence on UvrA (Chapman-Smith and Cronan, 1999). AFM was used to directly observe the UvrA-Qdot conjugates and to quantify the stoichiometry of biotinylated UvrA (UvrA-bio) binding to the streptavidin-coated Qdots at the single-molecule level. Qdots exhibit a homogeneous, symmetrical shape (Figure 1B). Since there are several streptavidin molecules attached to each Qdot (Qdot Streptavidin Conjugates User's Manual, Invitrogen), it was essential to find conditions that ensured the binding of only one UvrA dimer per Qdot. This was achieved by using a 5-fold excess of Qdots over UvrA-bio. After incubation of UvrA-bio with streptavidin-coated Qdots (Figure 1C), AFM images showed particles in close proximity to the Qdots (Figure 1C, orange arrow). Furthermore, statistical analyses of AFM images indicated that approximately 15% of the Qdots (n = 85) carried these particles, and no more than one particle was in close proximity to a Qdot.

To investigate whether or not UvrA-Qdot conjugates can still bind to DNA, agarose-based EMSAs were used in which Qdots and protein-Qdot conjugates can enter the gel matrix (Wang et al., 2008). EMSAs were performed with a 50 bp duplex DNA substrate containing a fluorescein-adducted thymine (Croteau et al., 2006) at the central position on the top strand (see Supplemental Information). A representative agarose gel assessing DNA binding of UvrA-bio before and after Qdot conjugation is shown in Figure 1D (right panel). Streptavidin-coated Qdots (in the absence of UvrA) did not interact with DNA (Figure 1D, left panel). UvrA- and UvrA-Qdot DNA complexes were clearly resolved under our agarose-EMSA conditions. At 20 and 50 nM protein concentrations, ~19% and 29% of the DNA was bound by UvrA-bio, respectively, which is comparable with results obtained using WT UvrA. After conjugation to Qdots, UvrA-Qdot bound to DNA to a similar extent as compared with unconjugated UvrA-bio (right panel of Figure 1D, compare lane 4 with 2 and lane 5 with 3). It is worth noting that under the same conditions, we observed 1:1 formation of UvrA-Qdot (Figure 1C). These results indicate that 1:1 conjugation of UvrA to Qdots does not significantly interfere with DNA binding by UvrA. In addition, EMSA assays also confirmed that conjugation of UvrA to a Qdot does not affect UvrB loading onto damaged DNA (Figure 1E, compare lane 7 with 6).

DNA Tightropes and the Interaction between Qdot-Labeled UvrA and DNA

To visualize the Qdot-labeled proteins, we constructed DNA tightropes (Figures 2A and 2B) by sequentially flowing through the construction materials as outlined in the Experimental Procedures (see Movie S2). Extended DNA was bound to 5 μm beads, elevating them from the surface, which not only prevented interactions of the Uvr proteins with the surface but also assisted in identifying when Uvr-Qdot proteins were bound. Any fluorescence in the focal region must derive from proteins bound to DNA and not the surface, which was out of the focal plane. Figure 2C shows the same region of tightropes as Figure 2B after the addition of 655 nm (red) Qdot-labeled UvrA. A number of red

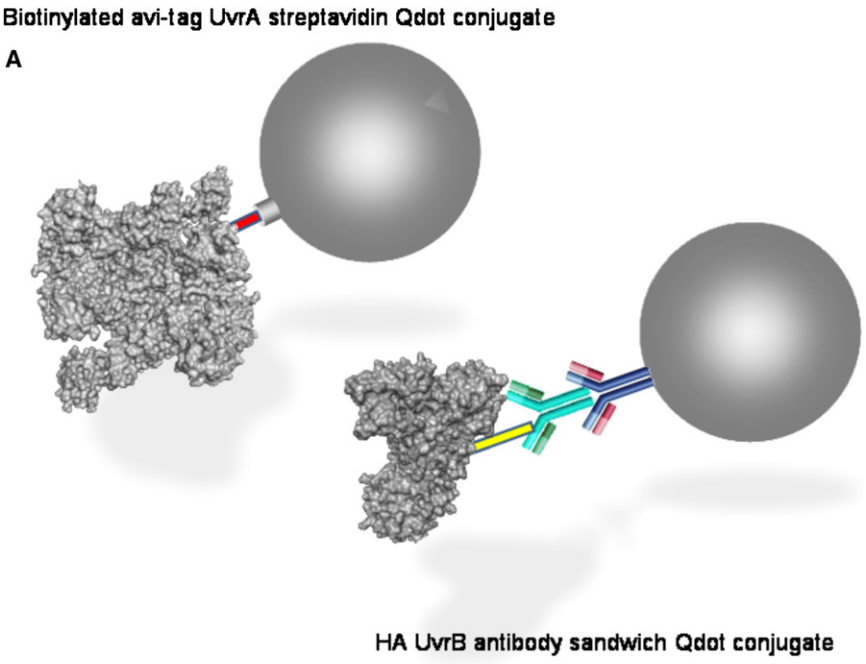

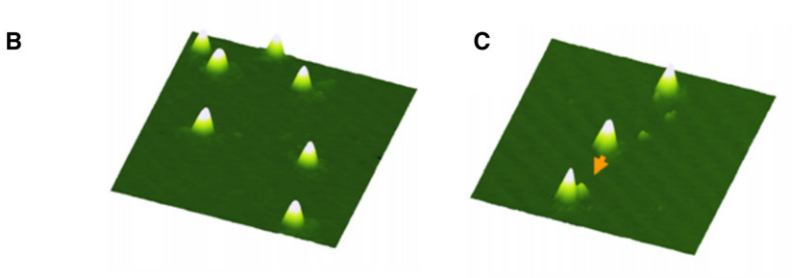

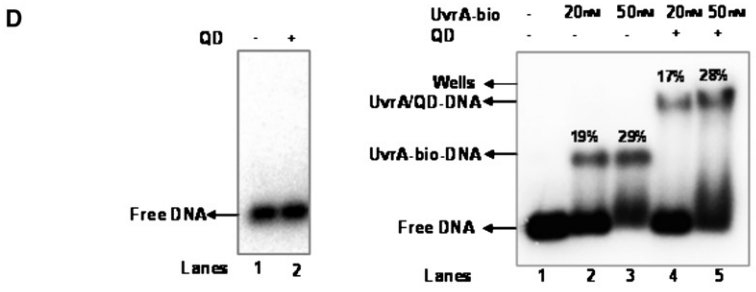

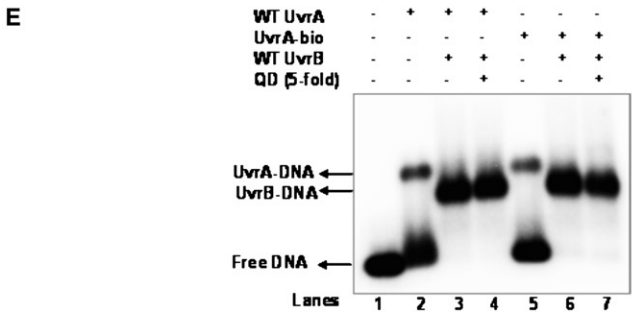

Figure 1. Qdot Labeling of UvrA and UvrB

(A) Attachment to UvrA was achieved through the biotinylation of UvrA using Avitag technology (see Supplemental Information) to which a streptavidin-coated Qdot was attached. For UvrB, we employed an antibody sandwich to distinguish the labeling strategies, thus permitting the inclusion of both labeled proteins in the same assay without crosstalk.

(B and C) AFM images of streptavidin-coated Qdots alone (B) and Qdots in the presence of UvrA-bio (C). Orange arrow points to a UvrA conjugated to a Qdot. The AFM image sizes are 400 × 400 nm at 15 nm height scale.

(D) Qdots do not bind to DNA (left). The addition of Qdots had no effect on the migration through an agarose gel of the target DNA. On the right, EMSA shows binding of UvrA and UvrA-Qdots to a fluorescein-containing DNA substrate where fluorescein serves as a lesion.

(E) EMSA showing that conjugation of UvrA to a Qdot does not affect its ability to load UvrB.

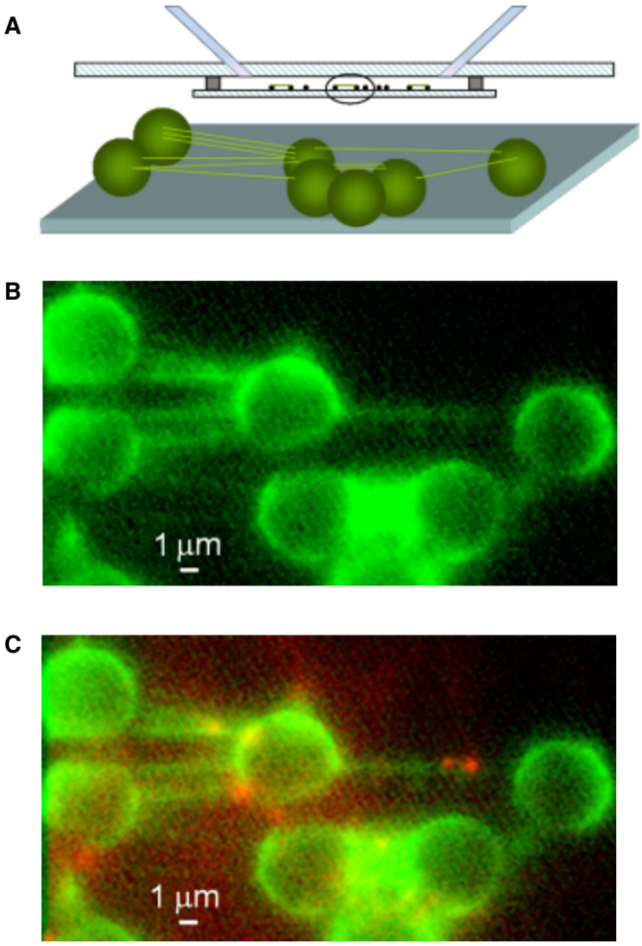

Figure 2. Experimental Layout of DNA Tightropes within a Flowcell

(A) A cross-section of the flowcell showing the placement of the inlet and outlet tubes into a standard microscope slide. A syringe pump attached to the tubes was used to withdraw solutions placed into an external reservoir; this permitted solution changes to be made rapidly and easily without disruption to flow. The tightropes were assembled in situ by the successive addition of the components required (see Experimental Procedures). Once assembled and washed, Qdot-labeled proteins could be introduced. During experiments, no flow was applied. In the lower panel, a 3D representation of a series of DNA tightropes is shown.

(B) Actual image of the surface (scale bar represents 1 μm) clearly showing the DNA tightropes labeled with YOYO-1 dye.

(C) Imaging UvrA bound to DNA. The same sample region from Figure 2B is shown after UvrA-$Qdot_{655}$ has been introduced to the flowcell. UvrA binding is clearly seen as red spots on the green DNA strands.

fluorescent spots appear on the DNA, each corresponding to a single UvrA molecule conjugated to a Qdot (Movie S3). As a control, Qdots were not observed to attach to the DNA in the absence of conjugation to UvrA (data not shown).

The experimental approach developed here results in the binding of numerous Uvr protein-conjugated Qdots throughout the visual field (x,y coordinate) at any point in time. To characterize all potential binding events throughout the entire visual field, we developed a simple "streak analysis" that assessed both the duration and mode of binding. This method of data presentation involves taking an intensity profile along a specified line through every frame in the movie, hence creating a movie of kymographs (described in Supplemental Information and Movie S4).

Briefly, this very simple transposition of the data set dimensions (x,y space through time is converted to x,t space through y increments) permits an extremely simple, rapid, and accurate analysis of the data from many molecules. Measuring the lengths of the lines, "time streaks" associated with the appearance and disappearance of a Qdot in each frame provide the lifetime of the interaction between the Qdot-labeled molecule and DNA. In addition, since the DNA is reasonably well aligned to the horizontal axis of the frame, any Qdot motions along the DNA will result in nonhorizontal streaks, yielding information about movement. Directed motion appears as a sloped time streak, whereas unbiased random walks appear as undulating time streaks (see Figure 3A for example time streaks).

Figure 3B shows the duration of interaction for 337 UvrA molecules in three separate experiments obtained from streak analysis of horizontal time streaks (Figure 3A, top panel), which is indicative of a bound, nonmotile UvrA. The lifetimes were binned and plotted as a histogram to reveal an exponential character expected for a single stochastic process that limits release of the molecule from the DNA. A second exponential is also seen; however, due to its very small amplitude, it was not examined further in this study. From this analysis, the rate of detachment from the DNA is 0.14 (± 0.01) s^{-1}, equivalent to a residence time of ~7 s.

Surprisingly, very few of the UvrA encounters with DNA (less than 5%) exhibited any motion, i.e., nonhorizontal time streaks. Qdots were considered motile if their corresponding time streaks showed at least one clear change in position; based on these criteria, ~5% of streaks showed movement. However, less than 1% of molecules showed any clear continuous motion on the DNA. Despite this lack of sliding, we observed UvrA molecules jumping from one DNA duplex to another without an apparent return to bulk solution (Movie S5). Qdot positions were tracked using the MTrackJ (ImageJ plugin). It is interesting to note that this intermolecular "jumping" did not require the two DNA helices to be in direct contact, with a resulting mean translocation distance of 1.2 (± 0.1 SEM [steps]) μm (n = 51 molecules and 190 steps). Long-range translocations were scored when a Qdot disappeared and then reappeared in the next frame (t = 483 ms). The low concentration of UvrA-Qdots in these experiments makes the binding of a different UvrA molecule from the solution pool unlikely (see calculation in Supplemental Information). Indeed, no differences in the total incidence of UvrA jumping from one DNA strand to another were apparent with flowcells that had all free UvrA flushed from the flowcell.

Stoichiometry of UvrAB Interactions

Given the unique dual-color labeling strategy employed here, we were able to address a key question in the field: the stoichiometry of the UvrAB interaction. First, we evaluated the oligomeric states of UvrAB by capturing complexes formed in the absence of DNA on a surface and then imaging using total internal reflectance fluorescence microscopy (TIRFM). We observed very few colocalized red ($Qdot_{655nm}$) and green ($Qdot_{565nm}$) Qdots (2.7%)

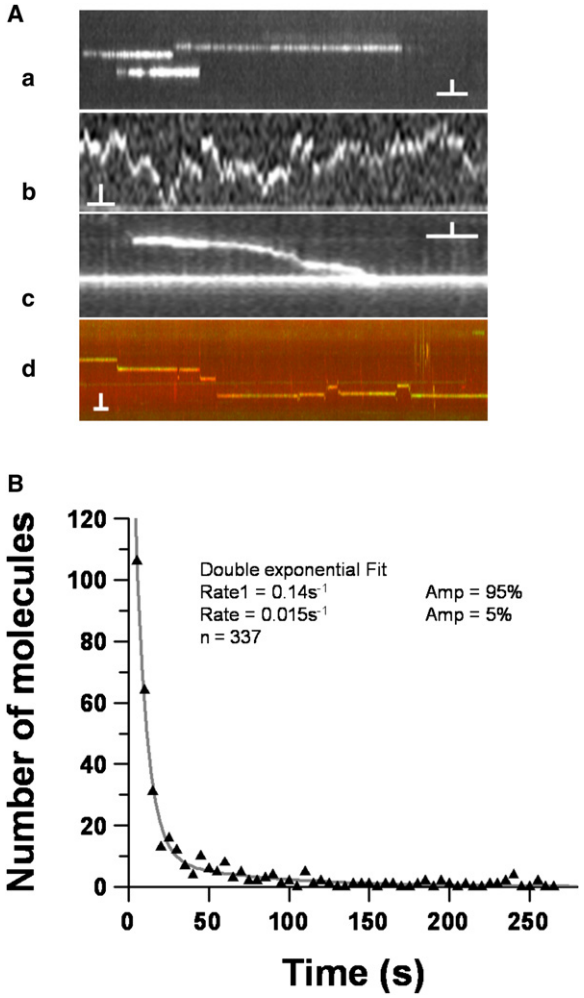

Figure 3. Analyzing the Binding of Uvr-Qdot Proteins to DNA Tightropes

(A) Kymographs of UvrAB complexes in motion. Four kymographs (a–d) are shown; these are unprocessed displacement versus time plots taken directly from the image files. Kymographs b–d originate from Movies S6–S8, respectively. Each vertical scale bar represents 1 μm (in subpanel d, 2 μm) and horizontal 5 s (in subpanel d, 10 s). Subpanel a shows a kymograph of a statically attached protein-Qdot to the DNA; the length of the "time streak" corresponds to the attached lifetime. Subpanel b shows unbiased free diffusion of the Uvr-Qdot protein complex corresponding to Movie S6. Subpanel c shows an example of Uvr-Qdot protein molecule with a directional bias to its diffusion (top trace), corresponding to Movie S7. Subpanel d shows an example of "paused motion," where molecules exhibit long pauses during their motion, corresponding to Movie S8. The total number of observations was 1221; 213 showed movement, and 1008 were static.

(B) The lifetime of UvrA binding to DNA. The lifetimes of 337 UvrA-Qdot molecules with characteristic horizontal time streaks across multiple experiments are plotted as a histogram and fitted to a double exponential, consistent with two Poisson processes. Given the very low amplitude of the second process (5%), we have ignored this in further analyses. The 95% amplitude signal indicates a detachment rate of 0.14 (± 0.01) s^{-1}. Therefore, on average, UvrA remains bound for ~7 s.

in the absence of protein (Table 1). We labeled UvrB with red and green Qdots such that only one Qdot was bound per protein molecule; in the absence of UvrA, we saw little colocalization

Table 1. Stoichiometry of UvrAB Complexes

			Number of Observations		
Proteins	DNA	Qdot Label	Red	Green	Yellow[b]
-	–	Alone[c]	3223	464	26 (2.7%)[d]
UvrB	–	UvrB	1738	404	74 (7.7%)[d,e,f]
UvrA + UvrB	–	UvrB	454	270	197 (21%)[e]
UvrA[a]	+	UvrA	115	67	127 (33%)
UvrA + UvrB	+	UvrB	56	37	38 (25%)[f]

The stoichiometry of UvrAB complexes was determined in the presence and absence of DNA. The latter was achieved by introducing a sample preincubated with excess $Qdot_{565}$ (green) and $Qdot_{655}$ (red) into a flowcell followed by immediate wash-through of buffer. This was performed to prevent surface saturation with Qdots and to ensure that the proteins bound to the surface reflected the population that was initially present when the sample was flowed in. Due to the large dilution upon introduction to the flow-chamber, the lack of a wash-though would provide a time-averaged view of the sample that would show a greater number of monomers. With DNA tightropes, this was not necessary, since the DNA was elevated from the surface, resulting in a lower background, and the dilutions were not excessive. The large excess of red over green Qdots was due to the experimental procedure where Qdots visible in the red channel were used as a cue to begin recordings. Given this large excess of red Qdots, we calculated an upper estimate of the percent yellow population in our controls by generating a total population from the number of green Qdots only, thus preventing our data being skewed by the greater number of red Qdots.

[a] Zero ATP.

[b] Percentage of yellow relative to the total Qdots capable of forming a complex (i.e., 2 × green + 2 × yellow) shown in parentheses.

[c] No Qdots bind to DNA in the absence of Uvr proteins.

[d] Significantly different (chi-square test: $p < 0.001$).

[e] Significantly different (chi-square test: $p < 0.001$).

[f] Significantly different (chi-square test: $p < 0.001$).

(7.7%). However, in the presence of UvrA, UvrB formed dual-colored complexes (21%), indicating that UvrA facilitates the formation of a complex containing two molecules of UvrB. We also studied the formation of complexes on DNA tightropes; both UvrA individually and UvrB (in the presence of UvrA) formed dual-colored complexes on DNA (33% and 25%, respectively). These data indicate that under the conditions of our experiments, UvrB is mostly a monomer, and two independent molecules can bind to a UvrA dimer to form a $UvrA_2B_2$ complex. This is in agreement with bulk methods using FRET (Malta et al., 2007) and is consistent with the recent structures of the UvrA-UvrB interface domains (Pakotiprapha et al., 2008, 2009).

The Effect of UvrB on the Binding of UvrA to DNA

Based on the dwell time data of UvrA alone and the known inefficiency of 3D searching (Halford and Szczelkun, 2002; Slutsky and Mirny, 2004; von Hippel and Berg, 1989), it would appear that UvrA is incapable of sampling ample genomic DNA prior to bacterial cell division (for calculations, see Supplemental Information). We therefore sought to assess the effects of its known binding partner UvrB. UvrB could increase UvrA's rate of DNA sampling by two methods: (1) reduce the

dwell time spent at any one site, or (2) collapse the 3D search into a 1D search.

We have previously shown that Qdot-conjugated UvrB interacts with and can be loaded onto DNA by UvrA (Wang et al., 2008). To ascertain that the same interaction exists in our present experimental system, we performed a simple control experiment: Qdot-conjugated UvrB was incubated with or without Qdot-conjugated UvrA before being loaded into the flowcell. UvrB-conjugated Qdots were observed to bind to the DNA only when UvrA was present (data not shown). Additionally, in a dual-color experiment, red Qdot-conjugated UvrB was observed to load onto DNA preloaded with green UvrA-Qdot, suggesting the preformation of UvrAB complexes in solution was not essential. Lastly, even in the absence of DNA, UvrA was seen to coordinate the association of two UvrB molecules to form the UvrAB complex (Table 1). These observations confirm that Qdot-conjugated UvrB interacts with Qdot-conjugated UvrA.

To determine how UvrB alters the binding of UvrA to DNA, we applied two complementary approaches using untagged and Qdot-conjugated wild-type UvrB. Both approaches gave identical rates, and these data were therefore combined. Figure 4A shows a histogram of UvrA interactions in the presence of UvrB. No apparent change in the rate of detachment was observed (0.14 s^{-1} versus 0.13 s^{-1}). To further assess how UvrB affects UvrA's interaction with DNA, we performed a titration of UvrB against a constant concentration of UvrA. Figure 4B shows a compilation of rates derived from exponential fits to lifetime histograms similar to that shown in Figure 4A at differing UvrB concentrations. Interestingly, the apparent rate of UvrA's detachment from DNA was not increased by the presence of UvrB. While these data suggest that UvrB does not influence the off rate of nonmoving UvrA molecules from DNA, we did detect a remarkable change in the number of motile protein molecules (see below). When the lifetimes of only these motile complexes were examined in isolation, an increase in the residence time on DNA to ~40 s was revealed (Figure 4C).

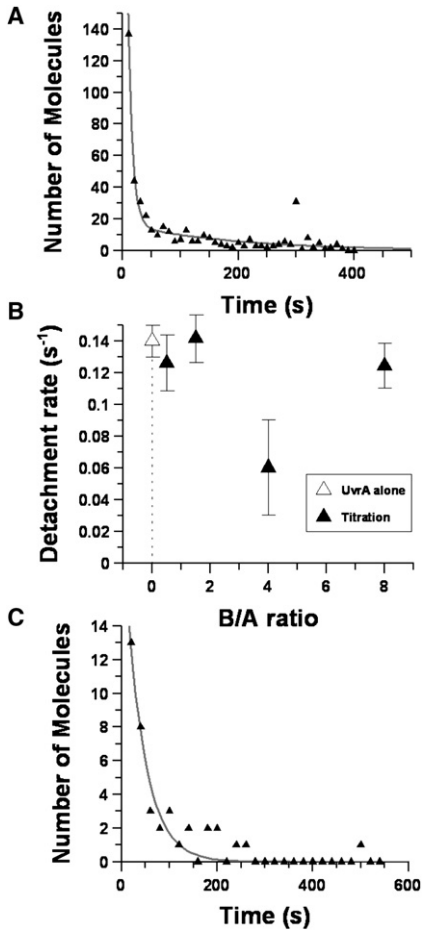

Figure 4. The Effects of UvrB on UvrA's Interaction with DNA

(A) Lifetime of UvrA-Qdot binding with UvrB present. The lifetimes of 449 molecules (with only UvrA labeled) across multiple experiments are plotted and fitted to a double exponential. As with UvrA alone, one process had a very low amplitude (<5%) and hence was ignored in further analyses. The larger amplitude signal indicates a detachment rate of 0.13 (± 0.02) s^{-1}. This difference is not sufficient to suggest an effect of UvrB binding on the attached lifetime of UvrA.

(B) Effect of different concentrations of UvrB on the detachment rate of UvrA. The analysis in (A) was performed across a range of UvrA/UvrB ratios, fixing the concentration of UvrA. Error bars are derived from exponential fits to lifetime histograms at the indicated UvrA/UvrB ratio.

(C) The attached lifetime of motile UvrAB complexes. UvrB was found to induce the motility of UvrA in the UvrAB complex (see main text). The lifetimes of complexes identified to be moving were plotted as a histogram and fit to a single exponential decay, yielding a detachment rate of 0.025 (± 0.003) s^{-1}, equivalent to an average lifetime of 40 s.

The Motion of UvrAB Complexes on DNA

In the presence of UvrB, UvrA exhibited a statistically significant (chi-square test; $p < 0.001$) 3-fold higher probability of movement (~17% versus ~5%), suggesting that the UvrAB complex is more motile. Of 1221 observed interactions between UvrAB complexes and DNA, 213 (17%) moved greater than 125 nm (one pixel), and 1008 remained static, representing a large increase in the number of motile complexes versus UvrA alone. Of these motile complexes, 36 of their time streaks were of sufficient duration (at least five frames) to be analyzed in detail. We noted three types of motion (Figure 3A): (1) 61% of the motile molecules showed free diffusion (n = 22), where the protein-Qdot complex varied randomly in position (Figure 3Ab and Movie S6); (2) 19% of the motile molecules showed directed motion (n = 7), where the protein-Qdot complexes were observed to possess directionality and hence were sloped (Figure 3Ac [top molecule] and Movie S7); and (3) 19% of the motile molecules displayed paused motion (n = 7), which was characterized by long pauses followed by short bursts of movement (Figure 3Ad and Movie S8). The mean squared displacement (MSD) of each freely diffusing UvrAB complex (category one) was plotted against time in Figure 5A. The average slope provided the diffusion constant calculated as 4.4 (± 0.2) × 10^{-4} $\mu m^2 s^{-1}$.

The second and third categories of motile molecules demonstrated a bias to their motion, consistent with directed motion or motion under flow. There was no imposed flow during observations, and the direction of the movement did not necessarily correlate with the former flow direction. Therefore, it is likely that the mode of binding is altered to facilitate directed

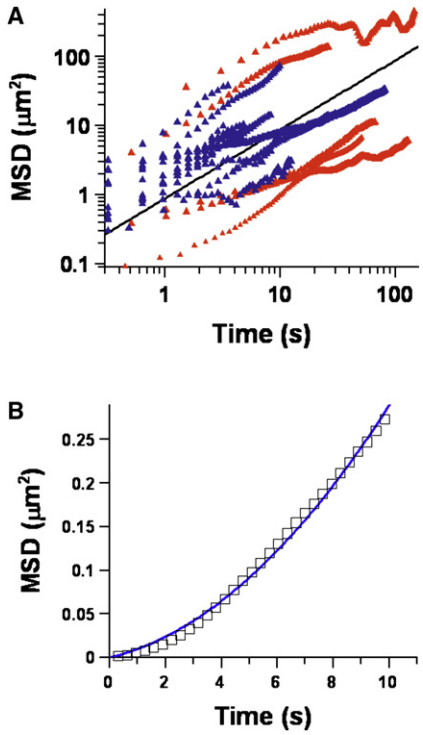

Figure 5. The Multiple Modes of UvrAB Complex Motion

(A) Mean squared displacement (MSD) plot of UvrAB complexes diffusing. The MSD was determined by calculating the squared distance moved during a prescribed time window. All data for that size window were averaged to produce a single point on the graph. The time window size was incrementally increased and the analysis reiterated to generate the time dependence of the mean displacement squared. The linear relationship is characteristic of unbiased diffusion. Data in blue represent each UvrA molecule (in the UvrAB complex) examined, and red represents the data originated from a dual-colored UvrAB complex. A log-log representation was used because the data were spread over orders of magnitude in time and displacement. A single origin-fixed linear regression gave a diffusion constant of 4.4 (± 0.2) × 10^{-4} $\mu m^2 s^{-1}$. (B) Representative MSD plot for a molecule exhibiting directed motion. The mean squared displacement for a Qdot-labeled UvrAB complex with clear directed motion shows characteristic upward curvature when plotted with linear axes (in log-log space, a straight line with slope = 2 would be observed). These data were fit to a second order polynomial, the linear term revealed the unbiased diffusive component, and the quadratic term revealed the directed component. For this molecule, the values were 7.7 (± 0.7) × 10^{-3} $\mu m^2 s^{-1}$ and 2.1 (± 0.1) × 10^{-3} $\mu m s^{-1}$, respectively. The average diffusion for all of the data (n = 14) was 2.3 (± 1.2 SEM) × 10^{-3} $\mu m^2 s^{-1}$ and for the directed motion 1.3 (± 0.5 SEM) × 10^{-3} $\mu m s^{-1}$, equivalent to ~4 bps^{-1}.

motility. A representative MSD plot of this motion is shown in Figure 5B; the upward curvatures for all such plots were best fitted to a second-order polynomial. The coefficients of the quadratic and linear terms represent the velocity of directed motion and twice the 1D diffusion constant, respectively. From such fits, the mean rate of UvrAB complex-directed movement was 1.3 (± 0.5 SEM) × 10^{-3} $\mu m s^{-1}$ (~4 bps^{-1}) in addition to a mean unbiased diffusive component of 2.3 (± 1.2 SEM) × 10^{-3} $\mu m^2 s^{-1}$.

Paused motion (Figure 3Ad [bottom] and Movie S8) was not clearly correlated to the protein-labeling strategy used. When plotted as an MSD versus time, this motion showed curvature similar to that seen in Figure 5B; however, clearly not all upwardly curved plots showed paused motion. Furthermore, paused motion was not seen in those data possessing linear MSD plots (Figure 5A), consistent with free diffusion. To understand paused motion further, we simulated 100 unbiased diffusers with randomly located pauses exponentially distributed around a number of lifetimes. The average MSD plot from these simulations was linear, albeit with a reduced diffusion constant, giving no indication of the pauses contained in the data (see Supplemental Information). Therefore, MSD plot curvature associated with molecules undergoing paused motion is not due to pauses, indicating that the pauses occur preferentially in the directed-motion data set.

UvrAB Complex Motility in the Absence of ATP

The current models for bacterial NER suggest an important role for ATP in UvrA dimer formation that increases UvrA's affinity for DNA (Goosen and Moolenaar, 2001). Furthermore, it is believed that ATP is absolutely required for productive UvrAB interaction and subsequent binding to a damaged site (Goosen and Moolenaar, 2001; Orren and Sancar, 1989; Truglio et al., 2006a). In this study so far, 1 mM ATP was used in all of the previous experiments with UvrB; therefore, we assessed the role of ATP by examining the binding of UvrA to DNA and the formation of UvrAB complexes in the absence of ATP. Consistent with previous work (Mazur and Grossman, 1991), in the absence of ATP, considerable static binding to DNA of UvrA was observed (data not shown). Furthermore, ATP was not required for the formation of dual-labeled UvrAB complexes or their subsequent association with the DNA. Thus, in contrast to bulk assays where the end points are productive, binding to a site-specific lesion in a DNA substrate, we found that ATP was unnecessary to form a UvrAB complex that is capable of binding to DNA. Also, in the absence of ATP, UvrAB was capable of motion unlike UvrA alone without ATP. It was found that 29% (± 1 SEM, n = 50 movers) of all imaged interactions showed some movement. Of all dual-labeled complexes containing one labeled UvrA and one labeled UvrB, 39% (± 0.3 SEM, n = 22 movers) showed movement in the absence of ATP. These data indicate that at the single-molecule level, ATP is apparently not required to form the UvrAB complex or for diffusively scanning DNA. It is possible, however, that some residual ATP may remain in the active sites of UvrA or UvrB. None of the moving molecules showed any directed motion, consistent with ATP acting as the energy source for this mode of motion, shown in Figure 5B.

DISCUSSION

The search for a lesion in DNA presents a considerable challenge to a repair system, since the damage site is tethered in a linear array and surrounded in three dimensions by nontarget DNA at very high local concentrations. This study sheds light on how the NER proteins UvrA and UvrB address this problem. By using a unique DNA tightrope assay that permits direct visualization of the interaction of a large ensemble of these Qdot-conjugated proteins with DNA, we have shown that UvrA forms a dimer

that is capable of bringing together two UvrB molecules both on and off DNA. On DNA, the association with UvrB switches the UvrAB search mechanism so that a much larger proportion of molecules participate in a 1D diffusional search. These observations have uncovered another damage recognition role for UvrB, which is to activate sliding on DNA. By individually labeling UvrA with one color Qdot and UvrB with a second color, we have directly visualized complex formation and composition in real time (Movie S9).

UvrB Affects How UvrA Interacts with DNA

Without UvrB present, UvrA employs a 3D random search mechanism, where it binds DNA for ~7 s before releasing and rebinding elsewhere. UvrA was also found to jump a mean distance of 1.2 μm between DNA molecules without returning to bulk solution, offering an alternative mechanism for accelerating the rate of diffusional encounter. This compares well to a previous study imaging the motion of EcoRV (Bonnet et al., 2008), but is in contrast with the few other enzymes examined using single-molecule techniques and that are known to utilize a 1D search mechanism (Blainey et al., 2006; Gorman et al., 2007; Kabata et al., 1993; Tafvizi et al., 2008).

The interaction of UvrAB with DNA becomes more complicated since both nonmotile and motile complexes were observed. The residence time of the former on DNA remained at ~7 s regardless of the ratio of UvrB to UvrA. This important observation suggests that UvrB does not alter the mechanism of UvrA's detachment from DNA. Conversely, the observed motile UvrAB complexes exhibited a 6-fold increase in their residence time on DNA. Therefore, UvrB changes UvrA's mode of interaction from a nonmotile to a sliding molecule and at the same time alters how the UvrAB complex dissociates from DNA. It is important to note that for successful analysis of sliding velocities, we could only examine the longer records, biasing our assessment to longer lifetimes; therefore, the 6-fold increase in attached lifetime is an upper estimate. Nonetheless, a change in mode and mechanism of UvrA's interaction with DNA is evident. However, why only a fraction (17%) of the molecules enter a search mode is unclear at present. It is possible that the binding equilibrium between UvrA and UvrAB is not saturated; however, no clear correlation was observed between the ratio of UvrB to UvrA and the number of motile molecules in Figure 4B (data not shown).

For those molecules that enter a search mode, we calculated the diffusion constant from a linear fit to the MSD versus time plot yielding 4.4×10^{-4} $\mu m^2 s^{-1}$. The maximum theoretical diffusion constant for Qdot-labeled UvrAB complex (Stokes radius of ~13.5 nm) spiraling along the groove of DNA and therefore experiencing rotational as well as translational friction is calculated as 2.1×10^{-2} $\mu m^2 s^{-1}$ (Schurr, 1979). This value is ~50-fold greater than our observed value, indicating that the UvrAB complex encounters large energy barriers to free motion. We have calculated the energy barrier assuming the UvrAB complex steps by 1 bp along the DNA as 3.9 $\kappa_B T$ (see Supplemental Information). This energy barrier is considerably higher than the predicted 2 $\kappa_B T$ for efficient target location (Slutsky and Mirny, 2004). Although it is still possible that the complex is performing small "hops" to the next binding site (von Hippel and Berg, 1986, 1989), we assume these large barriers to motion exist as a consequence of the complex attempting to slide along the DNA. The high energy barrier to free sliding may be the result of the UvrAB complex causing significant structural alterations in the DNA as it scans for damage. Since the free energy barrier is 1.9 $\kappa_B T$ higher than efficient searching would predict (Slutsky and Mirny, 2004), it is necessary to recalculate how long it would take these complexes to scan a bacterial genome. Based on our observed diffusion constant of 4.4×10^{-4} $\mu m^2 s^{-1}$ for the Qdot-conjugated UvrAB complex, we calculate the distance scanned per encounter with the DNA for the UvrAB complex (after removing the Qdot contribution; see Supplemental Information) as ~2.5 kbp. Therefore, in order for the genome to be scanned, a single UvrAB complex in an *E. coli* cell would need to make ~1200 encounters with the DNA; if each encounter lasts 40 s, then the genome would be scanned in ~13 hr! Therefore, to scan the genome within the doubling time for *E. coli* at 37°C of 20 min, ~40 complexes would be required. This value is comparable to estimates for the number of complexes present in the cell. During the SOS response, more Uvr proteins are present and cell division is delayed, offering a greater opportunity to locate damage.

Comparison of UvrAB with Other DNA Repair Systems

It is of interest to compare the behavior of the damage recognition proteins involved in NER studied here using single-molecule motility assays with other repair proteins, including base excision repair glycosylases and mismatch repair proteins. T4 pyrimidine dimer glycosylase (PDG, formerly endonuclease V) has been shown to be highly processive at nicking DNA containing pyrimidine dimers, both in vitro and in vivo (reviewed in (Lloyd, 2005). These results would imply that T4 PDG, after acting on one pyrimidine dimer, is capable of sliding some distance to another dimer site. In addition, in vivo experiments with the UvrABC system suggested similar processivity (Lloyd, 2005). Recently, hOgg1 and Msh2-Msh6 have been examined using single-molecule approaches (Blainey et al., 2006; Gorman et al., 2007). Both systems exhibited much faster 1D diffusion constants (5.8×10^{-1} $\mu m^2 s^{-1}$ and 1.2×10^{-2} $\mu m^2 s^{-1}$, respectively), but also shorter interaction times than those reported here (0.025 and 10.2 s, respectively). Interestingly, despite these differences in diffusion constants and dwell times, the overall length of DNA scanned per encounter is similar between UvrAB, hOgg1, and Msh2-Msh6.

The UvrAB Complex Is Not Always Engaged in a Random Walk

In addition to the 1D diffusional motion, one-third of all the observed motile molecules in our study showed slow but directed motion. Quantitative examination of the motion of these molecules showed that the MSD plots did not accurately fit to a quadratic relationship, expected for directed motion, but instead fit well to a combination of 1D diffusion and directed motion. The combination of these two modes in one search strategy may be taken to mean that UvrAB diffuses between slow ~4 bp/s steps or, alternatively, may suggest a "burning bridges" Brownian ratchet model (Saffarian et al., 2004). While this motion could not increase the overall rate of the search, it

could help facilitate identification of a damaged site in the vicinity of the DNA encounter. UvrAB complexes were also observed to pause during their motion in a process termed here "paused motion." None of these pauses occurred during unbiased diffusion, but instead were limited to those molecules exhibiting directed motion. Furthermore, Monte Carlo simulations suggested that the paused motion did not generate the characteristic curvature of a directed mover. Therefore, paused motion may also represent a functional process associated with UvrAB complexes checking DNA for deformities associated with damage. Quantitative PCR data (Figure S1) suggest that the λ-DNA used in these experiments possess on average three sites of damage. These damaged sites may explain some of the heterogeneity of the motile complexes. Additionally, the macromolecular composition of the UvrAB complex may also contribute to the observed heterogeneity of protein motion. We have determined here that the UvrAB complex is largely $UvrA_2B_2$; however, some amount of $UvrA_2B$ is also likely to be present. We are currently engaged in linking the heterogeneity of these behaviors to both the complex composition and the presence of damage by incorporating damage into known regions of the DNA.

The Role of ATP

Through a large number of biochemical studies, it has been shown that both UvrA and UvrB consume ATP. While several hypotheses have been posited to explain the ATPase activity of UvrA and UvrB (Goosen and Moolenaar, 2001; Skorvaga et al., 2004; Truglio et al., 2006a), a definitive mechanism of action has not been realized. We find that by omitting ATP, UvrA was able to bind DNA in much the same manner as in the presence of ATP. This indicates that ATP is not necessary for binding of UvrA to DNA as previously suggested (Wagner et al., 2009). Furthermore, unlike previous bulk biochemical studies, UvrA was also capable of loading UvrB onto DNA in the absence of ATP. Therefore, our present studies indicate that ATP does not play a significant role in the association of UvrA or UvrAB with DNA. However, there was a substantial increase in the number of motile UvrAB complexes (from 17% to 29%) in the absence of ATP. As expected, in the absence of an external energy source, this motion did not appear directed. These data indicate that the presence of ATP alters the energy barriers to motion. One potential explanation of this is that ATP induces the helicase fold of UvrB to clamp down on the DNA, stalling further motion. Studies to investigate this are currently underway.

Structural Speculations on the Binding of UvrA and UvrAB to DNA

The NER mechanism is extremely versatile in its function, being able to remove a large variety of DNA adducts. The rich conformational complexity of the UvrAB proteins provides diverse interactions with DNA. We have found that UvrA binds to DNA as a dimer and displays no movement at the resolution of our experiments; however, UvrAB complexes are clearly more mobile on DNA. As discussed above, the energy barrier for a UvrAB complex making 1 bp steps along the DNA is 3.9 $\kappa_B T$. This energy barrier could be due to structural alterations in both the proteins and DNA. Indeed, the zinc fingers of UvrA are believed to make direct contact with the DNA (Croteau et al., 2006), and binding of UvrA to DNA causes a site-specific bend of 40–60°, as observed by atomic force microscopy (H.W. and B.V.H., unpublished data). This transient DNA bend at the site of the lesion may help facilitate opening of the DNA, allowing damage verification by UvrB (DellaVecchia et al., 2004). UvrB's helicase fold is coupled to a β-hairpin that makes direct contact with the DNA (Truglio et al., 2006b), which could be processing the DNA in an energy-requiring step during damage searching. Thus, we believe that the UvrAB complex dynamically samples the DNA's conformational state as it slides along the DNA. These motile UvrAB complexes would be expected to make fewer DNA contacts; therefore, it is surprising to note that they remain attached to the DNA for a longer period of time (40 s on average). Therefore, the decrease in the energy barrier to diffusing along the DNA is not reflected in a decrease of the energy barrier to detachment; rather, it would appear to show the opposite. To achieve this, UvrAB may form a ring around the DNA, such that with UvrB, UvrA binds more weakly but is topologically restrained from leaving the DNA. In high ionic strength conditions, UvrAB-Qdot complexes and also UvrA-Qdot alone were observed to slide rapidly along the DNA (0.25 [± 0.12] $\mu m^2 s^{-1}$; discussed in more detail in the Supplemental Information). The measured diffusion constants were greater than theoretically possible for rotational diffusion along the DNA groove. Therefore, the protein-Qdot complexes at high salt slide linearly along the DNA, ignoring the groove contour; this is consistent with the formation of a ring-like complex.

In summary, this study has demonstrated that UvrA can interact with DNA, forming nonmotile complexes with or without ATP (Figure 6 and Movie S10). This interaction does not efficiently search the genome and therefore may serve to keep UvrA within the vicinity of DNA. However, in the presence of UvrB, the central molecule of NER, the UvrAB complex becomes capable of performing a 1D search for damage as well as a 3D random binding search, greatly increasing the efficiency of locating lesions. With greater amounts of UvrB present during the SOS response, this mechanism links the activation of NER to the detection of DNA damage. We have found that the UvrAB complex employs multiple mechanisms in its 1D search, suggesting that there is considerable conformational flexibility in the Uvr damage search and recognition apparatus, perhaps underlying its ability to recognize structurally unrelated DNA adducts. Extending these studies to real-time imaging in the presence of DNA lesions and UvrC will permit a much clearer view of this complex mechanism. Indeed, given the similarities between UvrB and the eukaryotic NER protein XPD (Wolski et al., 2008), it is conceivable that the mechanisms revealed using this method of visualizing DNA-protein interactions will be shared across all families of life.

EXPERIMENTAL PROCEDURES

Experimental Conditions

All imaging experiments were performed in imaging buffer consisting of 50 mM Tris-HCl (pH 7.5), 50 mM KCl, 10 mM $MgCl_2$, 100 mM DTT, and 1 mM ATP (except in the minus-ATP experiments). The high DTT concentration prevented excessive photobleaching of the dye. This was preferred to oxygen scavenger systems used previously (Kad et al., 2003), since we have observed solution

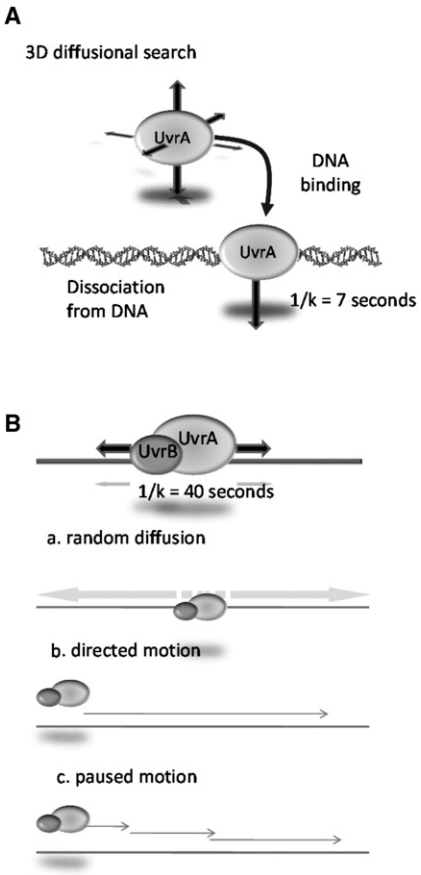

Figure 6. Summary of UvrA and UvrAB Motion

(A) UvrA (shown as a dimer) exhibits 3D searching with an average dwell time of 7 s on the DNA. UvrA can jump from one DNA molecule to another over long distances (~1 μm), but does not show any sliding.

(B) Of the UvrAB complexes on DNA, 17% showed movement. The movers had an average encounter time of 40 s and displayed three discrete types of motion: random diffusion, directed motion, and paused motion. Experiments presented here indicate that the UvrA dimer is capable of binding two independent UvrB molecules; however, the nature of the complex stoichiometry that underlies the different modes is unknown and currently under investigation. For an animated version of this figure, see Movie S10.

aggregates and incomplete elongation of the DNA under flow in their presence. DTT (100 mM) was confirmed by EMSA assays to have no effect on the formation of the preincision complex (data not shown). Qdots were used as described in the text and were always kept in excess to ensure only a single Uvr protein was attached to each Qdot (Wang et al., 2008). Experiments were performed at room temperature, and images were taken at various frame rates. Qdots were conjugated to UvrA through a streptavidin-biotin linkage and to UvrB through a HA-primary-secondary-Qdot sandwich (Supplemental Information).

DNA Tightrope Assay

Target site location for DNA repair proteins requires sorting through large stretches of nontarget DNA. In solution, DNA forms dynamic bundles (Movie S1), limiting visualization of protein-DNA interactions. Therefore, to investigate these properties, the DNA needs to be physically elongated, and this was achieved by suspending λ-DNA between 5 μm beads to form "DNA tightropes."

These tightropes were constructed using a flowthrough chamber (flowcell; see Supplemental Information) that allowed each solution to be passed over a polyethylene-glycol$_{5000}$ (PEG)-blocked surface. Despite this blocking, 5 μm poly-L-lysine-coated beads could randomly adhere to the PEG surface when passed into the flowcell. λ-DNA was subsequently flowed into the chamber for suspension between beads (Figure 2 and Movie S2). YOYO-1 dye was added after formation of DNA tightropes to facilitate locating the DNA strands in the field of view. Furthermore, this concentration of YOYO-1 dye was not found to affect the binding of UvrA and UvrB in ensemble assays. Figure 2B shows a typical visual field of DNA tightropes. Many adjacent tightropes are visible, creating a linear network of DNA akin to the high local concentrations of DNA present in vivo. Furthermore, this network permitted the observation of multiple DNA-protein interactions simultaneously. Another benefit of this assay is that there is no interaction between the DNA and the surface, which could interfere with the activity of the proteins. In addition, since flow was not imposed after setting up the tightropes, this enables detection of multiple modes of interaction, such as jumping from one DNA molecule to another and DNA sliding (Gorman and Greene, 2008). In many experiments, after confirming that the DNA molecules were attached to the beads, the YOYO-1 dye was washed free using 1XABC buffer.

Streak Analysis

To enable analysis of both dwell times of Qdot-labeled proteins and their modes of interaction with the DNA, we developed a process termed "streak analysis." This process consisted of three steps: (1) masking of bead pedestals, (2) event detection, and (3) data analysis (these are summarized in Movie S4).

Masking

To eliminate the contribution of Qdots bound to the poly-L-lysine-coated bead pedestals, we manually masked the 5 μm spheres from the field of view.

Event Detection

This approach consisted of creating kymograph time streak movies of the Uvr protein-Qdot conjugate interacting with λ-DNA strung between beads.

Data Analysis

These time streak movies were inspected frame by frame (i.e., in the y-dimension) to ascertain the period and the mode of binding. To address the effects of Qdot blinking, a streak was regarded as the same molecule if it disappeared and reappeared in the same location, since the probability of a binding event at the same location was considered negligible.

SUPPLEMENTAL INFORMATION

Supplemental Information includes Supplemental Experimental Procedures, Supplemental Data, Supplemental Calculations, Supplemental References, six figures, and ten movies and can be found with this article online at doi:10.1016/j.molcel.2010.02.003.

ACKNOWLEDGMENTS

We thank Samantha Beck for technical assistance, Andrew Dunn for discussions and measurements of flow rates, and M.D. Yusuf Ali and the rest of the Warshaw lab for critical discussions. We also thank Susan Wallace and Alan Chant at the University of Vermont for their crucial support in the early stages of this project. We thank Dorothy Erie at the University of North Carolina at Chapel Hill for her suggestions and AFM instrument time, and we also thank Harshad Ghodke for help in preparing some of the proteins used in this study. Finally, we wish to thank the reviewers for their very helpful suggestions that improved the quality of this study. This work was supported by NIEHS/NIH intramural program, UPCI-startup (B.V.H.), DB007A7 (N.M.K.), The Royal Society (DB3HR6 to N.M.K.), and National Institutes of Health Grants HL059408, HL085489 (D.M.W.), and K99ES016758-01 (H.W.).

Received: July 8, 2009
Revised: October 14, 2009
Accepted: December 23, 2009
Published: March 11, 2010

REFERENCES

Batty, D.P., and Wood, R.D. (2000). Damage recognition in nucleotide excision repair of DNA. Gene *241*, 193–204.

Blainey, P.C., van Oijen, A.M., Banerjee, A., Verdine, G.L., and Xie, X.S. (2006). A base-excision DNA-repair protein finds intrahelical lesion bases by fast sliding in contact with DNA. Proc. Natl. Acad. Sci. USA *103*, 5752–5757.

Bonnet, I., Biebricher, A., Porté, P.L., Loverdo, C., Bénichou, O., Voituriez, R., Escudé, C., Wende, W., Pingoud, A., and Desbiolles, P. (2008). Sliding and jumping of single EcoRV restriction enzymes on non-cognate DNA. Nucleic Acids Res. *36*, 4118–4127.

Caron, P.R., Kushner, S.R., and Grossman, L. (1985). Involvement of helicase II (uvrD gene product) and DNA polymerase I in excision mediated by the uvrABC protein complex. Proc. Natl. Acad. Sci. USA *82*, 4925–4929.

Chapman-Smith, A., and Cronan, J.E., Jr. (1999). The enzymatic biotinylation of proteins: a post-translational modification of exceptional specificity. Trends Biochem. Sci. *24*, 359–363.

Croteau, D.L., DellaVecchia, M.J., Wang, H., Bienstock, R.J., Melton, M.A., and Van Houten, B. (2006). The C-terminal zinc finger of UvrA does not bind DNA directly but regulates damage-specific DNA binding. J. Biol. Chem. *281*, 26370–26381.

DellaVecchia, M.J., Croteau, D.L., Skorvaga, M., Dezhurov, S.V., Lavrik, O.I., and Van Houten, B. (2004). Analyzing the handoff of DNA from UvrA to UvrB utilizing DNA-protein photoaffinity labeling. J. Biol. Chem. *279*, 45245–45256.

Friedberg, E.C., Walker, G.C., and Siede, W. (1995). DNA repair and mutagenesis (Washington, DC: ASM Press).

Friedberg, E.C., Walker, G.C., Seide, W., Wood, R.D., Schultz, R.A., and Ellenberger, T. (2006). DNA Repair and Mutagenesis (Washington, DC: ASM Press).

Goosen, N., and Moolenaar, G.F. (2001). Role of ATP hydrolysis by UvrA and UvrB during nucleotide excision repair. Res. Microbiol. *152*, 401–409.

Gorman, J., and Greene, E.C. (2008). Visualizing one-dimensional diffusion of proteins along DNA. Nat. Struct. Mol. Biol. *15*, 768–774.

Gorman, J., Chowdhury, A., Surtees, J.A., Shimada, J., Reichman, D.R., Alani, E., and Greene, E.C. (2007). Dynamic basis for one-dimensional DNA scanning by the mismatch repair complex Msh2-Msh6. Mol. Cell *28*, 359–370.

Granéli, A., Yeykal, C.C., Robertson, R.B., and Greene, E.C. (2006). Long-distance lateral diffusion of human Rad51 on double-stranded DNA. Proc. Natl. Acad. Sci. USA *103*, 1221–1226.

Halford, S.E., and Szczelkun, M.D. (2002). How to get from A to B: strategies for analysing protein motion on DNA. Eur. Biophys. J. *31*, 257–267.

Husain, I., Van Houten, B., Thomas, D.C., Abdel-Monem, M., and Sancar, A. (1985). Effect of DNA polymerase I and DNA helicase II on the turnover rate of UvrABC excision nuclease. Proc. Natl. Acad. Sci. USA *82*, 6774–6778.

Kabata, H., Kurosawa, O., Arai, I., Washizu, M., Margarson, S.A., Glass, R.E., and Shimamoto, N. (1993). Visualization of single molecules of RNA polymerase sliding along DNA. Science *262*, 1561–1563.

Kad, N.M., Rovner, A.S., Fagnant, P.M., Joel, P.B., Kennedy, G.G., Patlak, J.B., Warshaw, D.M., and Trybus, K.M. (2003). A mutant heterodimeric myosin with one inactive head generates maximal displacement. J. Cell Biol. *162*, 481–488.

Karakas, E., Truglio, J.J., Croteau, D., Rhau, B., Wang, L., Van Houten, B., and Kisker, C. (2007). Structure of the C-terminal half of UvrC reveals an RNase H endonuclease domain with an Argonaute-like catalytic triad. EMBO J. *26*, 613–622.

Lehmann, A.R. (2001). The xeroderma pigmentosum group D (XPD) gene: one gene, two functions, three diseases. Genes Dev. *15*, 15–23.

Lloyd, R.S. (2005). Investigations of pyrimidine dimer glycosylases—a paradigm for DNA base excision repair enzymology. Mutat. Res. *577*, 77–91.

Machius, M., Henry, L., Palnitkar, M., and Deisenhofer, J. (1999). Crystal structure of the DNA nucleotide excision repair enzyme UvrB from Thermus thermophilus. Proc. Natl. Acad. Sci. USA *96*, 11717–11722.

Malta, E., Moolenaar, G.F., and Goosen, N. (2007). Dynamics of the UvrABC nucleotide excision repair proteins analyzed by fluorescence resonance energy transfer. Biochemistry *46*, 9080–9088.

Mazur, S.J., and Grossman, L. (1991). Dimerization of Escherichia coli UvrA and its binding to undamaged and ultraviolet light damaged DNA. Biochemistry *30*, 4432–4443.

Nakagawa, N., Sugahara, M., Masui, R., Kato, R., Fukuyama, K., and Kuramitsu, S. (1999). Crystal structure of Thermus thermophilus HB8 UvrB protein, a key enzyme of nucleotide excision repair. J. Biochem. *126*, 986–990.

Orren, D.K., and Sancar, A. (1989). The (A)BC excinuclease of Escherichia coli has only the UvrB and UvrC subunits in the incision complex. Proc. Natl. Acad. Sci. USA *86*, 5237–5241.

Orren, D.K., and Sancar, A. (1990). Formation and enzymatic properties of the UvrB.DNA complex. J. Biol. Chem. *265*, 15796–15803.

Pakotiprapha, D., Inuzuka, Y., Bowman, B.R., Moolenaar, G.F., Goosen, N., Jeruzalmi, D., and Verdine, G.L. (2008). Crystal structure of Bacillus stearothermophilus UvrA provides insight into ATP-modulated dimerization, UvrB interaction, and DNA binding. Mol. Cell *29*, 122–133.

Pakotiprapha, D., Liu, Y., Verdine, G.L., and Jeruzalmi, D. (2009). A structural model for the damage-sensing complex in bacterial nucleotide excision repair. J. Biol. Chem. *284*, 12837–12844.

Saffarian, S., Collier, I.E., Marmer, B.L., Elson, E.L., and Goldberg, G. (2004). Interstitial collagenase is a Brownian ratchet driven by proteolysis of collagen. Science *306*, 108–111.

Sancar, A. (1996). DNA excision repair. Annu. Rev. Biochem. *65*, 43–81.

Sancar, A., and Rupp, W.D. (1983). A novel repair enzyme: UVRABC excision nuclease of Escherichia coli cuts a DNA strand on both sides of the damaged region. Cell *33*, 249–260.

Sancar, A., and Sancar, G.B. (1988). DNA repair enzymes. Annu. Rev. Biochem. *57*, 29–67.

Schurr, J.M. (1979). The one-dimensional diffusion coefficient of proteins absorbed on DNA. Hydrodynamic considerations. Biophys. Chem. *9*, 413–414.

Skorvaga, M., DellaVecchia, M.J., Croteau, D.L., Theis, K., Truglio, J.J., Mandavilli, B.S., Kisker, C., and Van Houten, B. (2004). Identification of residues within UvrB that are important for efficient DNA binding and damage processing. J. Biol. Chem. *279*, 51574–51580.

Slutsky, M., and Mirny, L.A. (2004). Kinetics of protein-DNA interaction: facilitated target location in sequence-dependent potential. Biophys. J. *87*, 4021–4035.

Sohi, M., Alexandrovich, A., Moolenaar, G., Visse, R., Goosen, N., Vernede, X., Fontecilla-Camps, J.C., Champness, J., and Sanderson, M.R. (2000). Crystal structure of Escherichia coli UvrB C-terminal domain, and a model for UvrB-uvrC interaction. FEBS Lett. *465*, 161–164.

Tafvizi, A., Huang, F., Leith, J.S., Fersht, A.R., Mirny, L.A., and van Oijen, A.M. (2008). Tumor suppressor p53 slides on DNA with low friction and high stability. Biophys. J. *95*, L01–L03.

Takayama, K., Salazar, E.P., Broughton, B.C., Lehmann, A.R., Sarasin, A., Thompson, L.H., and Weber, C.A. (1996). Defects in the DNA repair and transcription gene ERCC2(XPD) in trichothiodystrophy. Am. J. Hum. Genet. *58*, 263–270.

Theis, K., Chen, P.J., Skorvaga, M., Van Houten, B., and Kisker, C. (1999). Crystal structure of UvrB, a DNA helicase adapted for nucleotide excision repair. EMBO J. *18*, 6899–6907.

Truglio, J.J., Rhau, B., Croteau, D.L., Wang, L., Skorvaga, M., Karakas, E., DellaVecchia, M.J., Wang, H., Van Houten, B., and Kisker, C. (2005). Structural insights into the first incision reaction during nucleotide excision repair. EMBO J. *24*, 885–894.

Truglio, J.J., Croteau, D.L., Van Houten, B., and Kisker, C. (2006a). Prokaryotic nucleotide excision repair: the UvrABC system. Chem. Rev. *106*, 233–252.

Truglio, J.J., Karakas, E., Rhau, B., Wang, H., DellaVecchia, M.J., Van Houten, B., and Kisker, C. (2006b). Structural basis for DNA recognition and processing by UvrB. Nat. Struct. Mol. Biol. *13*, 360–364.

Van Houten, B., Croteau, D.L., DellaVecchia, M.J., Wang, H., and Kisker, C. (2005). 'Close-fitting sleeves': DNA damage recognition by the UvrABC nuclease system. Mutat. Res. *577*, 92–117.

Verhoeven, E.E., Wyman, C., Moolenaar, G.F., and Goosen, N. (2002). The presence of two UvrB subunits in the UvrAB complex ensures damage detection in both DNA strands. EMBO J. *21*, 4196–4205.

von Hippel, P.H., and Berg, O.G. (1986). On the specificity of DNA-protein interactions. Proc. Natl. Acad. Sci. USA *83*, 1608–1612.

von Hippel, P.H., and Berg, O.G. (1989). Facilitated target location in biological systems. J. Biol. Chem. *264*, 675–678.

Wagner, K., Moolenaar, G., van Noort, J., and Goosen, N. (2009). Single-molecule analysis reveals two separate DNA-binding domains in the Escherichia coli UvrA dimer. Nucleic Acids Res. *37*, 1962–1972.

Wang, H., DellaVecchia, M.J., Skorvaga, M., Croteau, D.L., Erie, D.A., and Van Houten, B. (2006). UvrB domain 4, an autoinhibitory gate for regulation of DNA binding and ATPase activity. J. Biol. Chem. *281*, 15227–15237.

Wang, H., Tessmer, I., Croteau, D.L., Erie, D.A., and Van Houten, B. (2008). Functional characterization and atomic force microscopy of a DNA repair protein conjugated to a quantum dot. Nano Lett. *8*, 1631–1637.

Waters, T.R., Eryilmaz, J., Geddes, S., and Barrett, T.E. (2006). Damage detection by the UvrABC pathway: crystal structure of UvrB bound to fluorescein-adducted DNA. FEBS Lett. *580*, 6423–6427.

Wolski, S.C., Kuper, J., Hänzelmann, P., Truglio, J.J., Croteau, D.L., Van Houten, B., and Kisker, C. (2008). Crystal structure of the FeS cluster-containing nucleotide excision repair helicase XPD. PLoS Biol. *6*, e149.

Supplemental Information
Molecular Cell, *Volume 37*

Collaborative Dynamic DNA Scanning by Nucleotide Excision Repair Proteins Investigated by Single-Molecule Imaging of Quantum-Dot-Labeled Proteins

Neil M. Kad, Hong Wang, Guy G. Kennedy, David M. Warshaw, and Bennett Van Houten

Contents

1. Supplemental Experimental Procedures

1.1 Standard Buffer conditions

The standard buffer used in all experiments unless stated otherwise was termed ABC buffer and comprised: 50 mM Tris-HCl (pH 7.5), 50 mM KCl, 10 mM $MgCl_2$, 5 mM DTT, 1 mM ATP. Unless stated otherwise all experiments were performed at room temperature.

1.2 Protein purification

The biotin ligase recognition sequence GLNDIFEAQKIEWHEGGG (AviTag^{TM}), was added to the C-terminal of UvrA, using the forward primer (5′ GGC GTG CCA TGG CGA TGG CAT CAT CAA AAT TG 3′) and reverse primer (5′ CAA TAT GAA GCG GTG AAG GCG GGT CTG AAC GAC ATC TTC GAG GCT CAG AAA ATC GAA TGG CAC GAA GGT GGC GGT TGC TTT GCC AAG GGT ACC AAT G 3′). This resulted in the amplification of nucleotides 2211 to 2859 of the *uvrA* gene on pTYB1-Wt $uvrA_{bca}$ vector (Croteau et al., 2006). The PCR products were digested with KpnI and NcoI, gel purified, and cloned into the pTYB1-Wt uvrA^{bca} vector that

was also digested with same restriction enzymes. Insertion of the AviTag into the vector was confirmed by DNA sequencing. UvrA with AviTag (UvrA-avi) was purified using the IMPACT^{TM}-CN system (New England Biolabs) as described previously (Theis et al., 1999). After elution from the chitin column, UvrA-avi was dialyzed against a low salt buffer containing 50 mM Tris (pH 8.0) and 50 mM KCl. Biotinylation of UvrA-avi (160 μg) was performed in the presence of 2.5 μg of BirA biotin protein ligase (Avidity) at 30^{o}C overnight in a buffer containing 10 mM ATP and 50 μM biotin. Biotin protein ligase and extra biotin were removed from biotinylated UvrA-avi using a Vivaspin 500 column (Vivascience, MW cutoff 50 kDa). The extent of biotinylation of UvrA-avi was quantified using EZ^{TM} Biotin Quantitation Kit (Pierce). Cloning and purification of HA-tagged WT UvrB are described elsewhere (Wang et al., 2008). Proteins used in this study are greater than 95% pure as judged by the staining of SDS-PAGE protein gel with SimplyBlue^{TM} SafeStain (Invitrogen).

1.3 Atomic Force Microscopy

In preparing UvrA-Qdot conjugates, biotinylated UvrA (UvrA-bio, 25 nM) was incubated with Qdot 655 streptavidin conjugate (Invitrogen, 125 nM) in a buffer containing 50 mM Tris-HCl (pH 7.5), 50 mM KCl, and 10 mM $MgCl_2$ for 1 hour at ambient temperature. Immediately after a 5-fold dilution in the same buffer, samples were deposited onto freshly cleaved mica, rinsed with Nanopure deionized water and dried under a gentle stream of nitrogen gas. Sample preparation for UvrB-Qdot is described elsewhere (Wang et al., 2008). All images were collected using a Nanoscope IIIa microscope (Veeco Instruments) in oscillating mode. Pointprobe plus noncontact/tapping mode silicon probes with spring constants of ~50 N/m and resonance frequencies of ~190 kHz were used. Images were captured at a scan size of 1 μm × 1 μm, a scan speed of 3 Hz and a resolution of 512 × 512 pixels. AFM protein volumes were measured using Image SXM software (Ratcliff and Erie, 2001; Wang et al., 2008; Yang et al., 2003). Molecular weights were derived from AFM volume based on a standard linear curve: V=1.2 × (MW) - 15.5, where V is AFM volume and MW is molecular weight (Wang et al., 2008).

1.4 Electrophoresis Mobility Shift Assay (EMSA)

Electrophoresis mobility shift assays were performed using duplex DNA F50/NDB. The sequence of the top strand (F50) is 5′ GAC TAC GTA CTG TTA CGG CTC CAT CFC TAC CGC AAT CAG GCC AGA TCT GC 3′. F denotes a fluorescein adducted thymine. The top strand (F50) was radioactively labeled at the 5′ end and annealed with its complementary bottom strand (NDB) as described previously (Wang et al., 2006). UvrA-Qdot, WT UvrA, UvrA-bio, and WT UvrB were preheated (65°C, 10 min) separately prior to reactions. WT UvrA or UvrA-bio proteins (20 nM) were then incubated with Qdot 655 streptavidin conjugate (100 nM) in 1X ABC buffer at room temperature for 1 hour. Finally, duplex DNA (F50/NDB50, 2 nM), and WT UvrB (100 nM) were added when required. Reactions were further incubated at 37°C for 30 minutes. Half of the reaction volume was loaded onto a 1% agarose gel containing 1 mM ATP and 10 mM $MgCl_2$. Samples were subject to electrophoresis at 10 V/cm in a buffer containing 45 mM Tris (pH 7.5), 45 mM boric acid, 1.25 mM EDTA, 10 mM $MgCl_2$, and 1 mM ATP for 1 hour at 4°C, and then dried onto DE81 DEAE cellulose paper (Whatman). Gels were exposed to a PhosphorImager screen

(GE Healthcare) overnight, and scanned using a Typhoon™ 9400 Variable Mode Imager. Images were analyzed using ImageQuant 5.1 software. Reaction conditions for testing of the UvrB-QD using EMSAs are described elsewhere (Wang et al., 2008).

1.5 Quantitative PCR (QPCR)

Figure S1. QPCR Analysis of DNA Damage in λ DNA

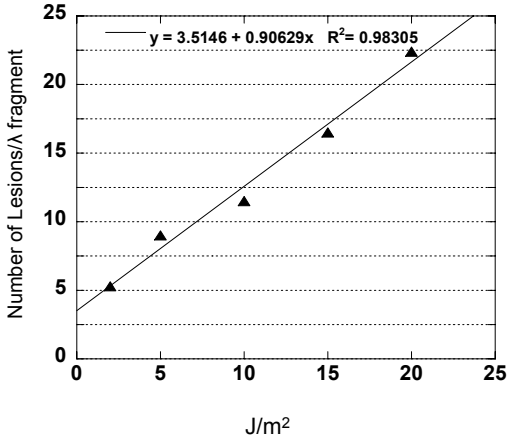

λ DNA (New England Biolabs) was diluted in TE buffer to a concentration of 50 μg/ml before UV-irradiation. UV exposures were achieved in a CL-1000 Ultraviolet Crosslinker (UVP) with an emission peak at 254 nm. The short target resides from nucleotides 32969 to 33174, and long target resides from nucleotides 26890 to 39488 on λ DNA template. The sequences of forward and reverse primers for amplifying the short target are: 5' GCA TAG CGA TTC AAA CAG GTG CTG 3', and 5' TTT TCC TAA TCA GCC CGG CAT TTC 3', respectively. The sequences of forward and reverse primers for amplifying the long target are: 5' CCA ACC ATC TGC TCG TAG GAA TGC 3', and 5' AGT TGG GTC CAC TTA TCG CGG AGT 3', respectively. The QPCR reactions were carried out and the lesion frequency was calculated as described previously (Meyer et al., 2007), except that λ DNA template was at 20 ng/ml. The cycling conditions for the short target are as follows: 75°C for 2 min; 94°C for 1 min; 94°C for 15 s, 64.5°C for 45 s, and 72°C for 30 s (20 cycles); and 72°C for 5 min. The cycling conditions for the large targets are: 75°C for 2 min; 94°C for 1 min; 94°C for 15 s and 66°C for 12 min (17 cycles); and 72°C for 10 min. Under the conditions listed, both primer pairs produced PCR products of expected length (assessed by agarose gel electrophoresis with ethidium bromide staining) using λ DNA as a template. Quantification of λ DNA template and PCR products concentration was performed using PicoGreen fluorescent DNA binding dye as described previously (Santos et al., 2006). **Figure S1** shows that damage increases linearly with exposure to UV; the y-axis intersect suggests that on average untreated λ-DNA possesses three lesions.

1.6 Flowcell construction

Figure S2. Schematic View of a Flowcell

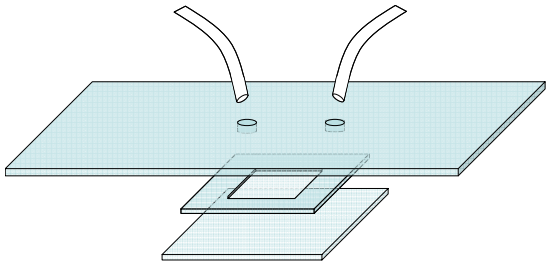

Flowcells were constructed by drilling two holes 15 mm apart through a standard glass microscope slide (Fisher finest) using a diamond bur (McMaster). Tubing (PE-60; Thomas Scientific) was passed through the holes and glued into place using UV curing adhesive (NOA68 Thorlabs). Once the tubes were fixed excess tubing was removed carefully using a scalpel blade. A gasket (Grace Bio Labs,

Inc., Bend, OR) was then applied to the sample side of the slide (see Figure S2). Coverslips (#1 Fisher finest) were pre-coated in $mPEG_{5000}$. This was achieved in three steps according to the procedure described in (van Oijen et al., 2003): (1) The coverslips were cleaned using NoChromix (Godax) and thoroughly washed; (2) the coverslips were then amine functionalized by soaking in 3-aminopropyl-triethoxysilane (Sigma Aldrich) in 2% dry acetone for 2 minutes followed by thorough washing with ddH_2O and a 30 min curing step at 110°C; (3) 10-20 μL 100 mg/mL methyl-polyethyleneglycol$_{5000}$-SPA (Lysan Biotech, AL) in 100 mM $NaHCO_3$ was dropped onto each coverslip surface and left to incubate in a humidor for 4 hours. The coverslips were washed and stored in the humidor. These coverslips were fixed to the adhesive gasket to create an enclosed disposable flowcell. Prior to experimentation flowcells were blocked for at least one hour and no longer than overnight with 10 mg/ml BSA, 0.1% Tween-20, 1 mM EDTA in 10 mM Tris pH7.5 at room temperature.

1.7 DNA tightrope construction and imaging

It was firstly necessary to prepare the surface beads for DNA attachment, 350 μg/mL poly-L-lysine (350 kDa Sigma) was introduced to washed 5 μm silica beads (Polysciences). After at least one hour a 25 μL aliquot of the bead-poly-L-lysine solution was removed and washed twice in a 20-fold excess of ddH_2O, using bench micro-centrifugation to separate beads from wash solution. These coated beads were taken up in 100 μL of ddH_2O, sonicated briefly and passed into a flowcell whilst examining bead density on the surface using a low magnification upright microscope. The correct density was empirically chosen such that an even spread of beads was seen throughout the flowcell. Once prepared the flowcells were then washed several times with 1X TE buffer.

Bead coated flowcells were then connected at one end to a syringe pump (WPI) and the other to a 1.5 mL centrifuge tubes drilled to permit access of pipette tips. By back-flushing with solution from the syringe it was possible to ensure no air was present in the system. The flowcell was again washed before 50 μL of 1.6 nM λ-DNA was pipetted into the holding tube prior to pumping into the flowcell. Once inside the flowcell the DNA was passed over the beads for at least ten minutes alternating direction every 100 μL at a flow-rate of 500 μL/min. After further washes, 1 nM of YOYO-1 dye in imaging buffer (1X UvrABC + 95mM DTT) was flowed into the flowcell to allow imaging of the DNA.
Protein-Qdot complexes were introduced into the flowcell after incubation in the conditions appropriate to the experiment. Below 0.25 nM UvrA it was difficult to observe binding of the complexes to the DNA, therefore labeled complexes were imaged at 0.5 nM and above. In addition, unlabeled (WT UvrA no biotin tag) was included with labeled UvrA to assist in dimer formation, therefore it was possible to image at very low concentrations of the UvrA-Qdot while ensuring that the UvrA could interact with the DNA. To ensure Qdots were only labeled with a single protein excess (2-5 fold) quantum dots were used. Based on previous (Wang et al., 2008) and current studies (see AFM section) these ratios were sufficient to ensure that the vast majority of quantum dots were singly labeled.

Images were acquired using a custom built total internal reflectance fluorescence (TIRF)-based instrument. The 488 nm line from a 50 mW Ar-ion laser (Spectra-Physics model 163) was selected using an AOTF (NEOS Technologies) and then expanded and guided into a Nikon TE2000-U microscope before being focused onto the back focal plane of a Nikon 100x 1.49NA objective lens. The beam was steered to the edge of the back aperture resulting in a highly inclined collimated light beam emerging from the objective. With a flowcell present this beam would totally internally reflect at the glass to water interface resulting in a near-field evanescent excitation wave at the flowcell surface. However to increase the penetration depth of the beam and to avoid excess background sample illumination the beam was adjusted to emerge at a sub-critical angle resulting in an obliquely angled fluorescence (OAF) illumination ray. To achieve this, the incident beam was steered off the edge of the objective's back aperture using a lens to defocus and steer the beam toward the center of the objective lens back aperture. This optic was mounted on an indexing mechanism that enabled the instrument to be easily switched between the TIRF and OAF modes of operation. Images were obtained using a Stanford Photonics XRmega10 1024x1024 ICCD camera (18000e^-/pixel). Dual color images were produced using a Dual View device (Optical Insights).

1.8 Data analysis

The movement of sliding non-static Qdots was measured using the ImageJ plugin spotTracker (Sage et al., 2005) and processed into MSD plots using a custom written VBA script within Microsoft Excel (available upon request).

Streak Analysis

The three steps used in streak analysis are outlined in more detail below:

Masking- To eliminate the contribution of Qdots bound to the poly-L-lysine coated bead pedestals, we manually masked the 5 μm spheres from the field of view. This was achieved by creating circular masks corresponding to the bead image using ImageJ. The poly-lysine coated beads were visible due to bound YOYO-1. Given the 565 nm channel filled exactly half of the visual image the mask drawn directly onto the 565 nm channel using the circular selection brush in ImageJ (NIH), and was then directly transposed onto and subtracted from the 655 nm image.

Event detection - This approach consisted of creating kymograph time streak movies of the Uvr protein-Qdot conjugate interacting with λ-DNA strung between beads. However, to detect the binding events throughout the three-dimensions (x, y, time) of the dataset we employed a variant of kymographic analysis. Typically kymographs are projections of a line throughout the time of the movie being analyzed. Such projections result in an image with the y-axis now representing time. This extremely useful method of analysis requires *a priori* knowledge of where in space and time the Qdots bind. Since our experimental approach can result in Qdots landing anywhere in the visual field we lacked this knowledge prior to analysis. To detect the binding events we therefore developed an approach where each horizontal line was scanned through time in successive single pixel increments down the y-axis. This produced a series of time-slices that were

subsequently stacked according to their vertical position into a movie, thus reordering the frame steps from time into y position (**Movie S4**). It was now possible to simply evaluate the intensity of every pixel in time and space throughout the dataset.

Data analysis – These time streak movies were inspected frame-by-frame (i.e. in the y-dimension) to ascertain the period and the mode of binding. Firstly, streaks were identified and measured; this provided the period of binding. To prevent potential duplication created by the blooming characteristics of the Qdot, every 'time-streak' identified in a 'space-frame' was compared to the preceding 'space-frame' and only counted once if present in both. Furthermore in this view of UvrA conjugated Qdot-DNA interactions, static binding of a simple on and then off event appeared as a straight horizontal line or streak through these data. Interactions involving sliding were observed as non-linear streaks. For example, directed motion would appear as a slope and diffusive motion would appear as a meandering line. For those DNA molecules not horizontally aligned the intensity of the line changed over the streak as the kymograph scans across the image of the Qdot. Normally this was not a problem in the analysis, however for molecules severely out of alignment we combined multiple frames looking for the maximum intensity in each using the GroupedZprojector plugin for ImageJ. Qdots are well known to blink, i.e. enter a dark-state. This presents problems for analysis of streaks, and despite strongly suppressing blinking using 100 mM DTT (Hohng and Ha, 2004), we still observe blinking. The probability that Qdots will land at the exact site of a previously bound Qdot in the visual field is lower than that calculated for UvrA hopping (see below); therefore we assume that any intermittent fluorescence in a streak represents blinking and therefore counts as the same molecule.

2. Supplemental Data

2.1 The effects of salt on binding and motion

To understand the physical mechanism by which UvrA and UvrAB interact with DNA we studied the effects of a number of NaCl concentrations on the detachment rate and binding. In these experiments, summarized in **Figure S3**, we altered the concentration of NaCl and introduced UvrA-Qdot. It is clear that the rate of detachment increases only slightly. By using a method developed to measure equilibrium p53 binding to DNA (Tafvizi et al., 2008), we were able to determine the amount of UvrA-Qdot bound at numerous NaCl concentrations. This method involved measuring the intensity of fluorescence for all regions in the DNA focal plane after masking the beads as described above. We performed this

Figure S3. The Effect of NaCl on UvrA Attachment to DNA

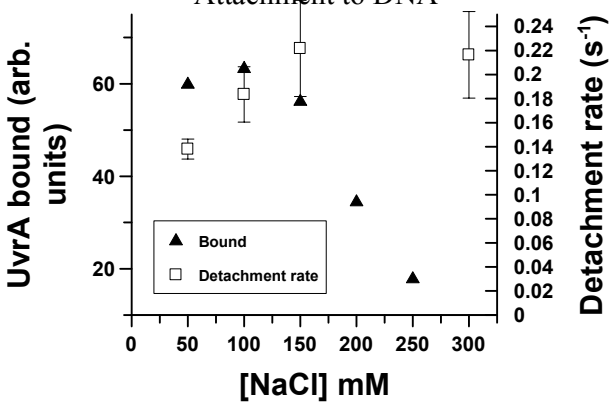

operation for movies of identical length and with solutions containing identical concentrations of UvrA-Qdot, which is important to normalize the background fluorescence. These data (Figure S3 - left axis) clearly show UvrA-Qdot binding decreases as the concentration of NaCl is increased. Since equilibrium binding is a measure of the ratio of attachment and detachment rates, the substantial effect of NaCl on binding is therefore primarily a result of a decreased attachment rate. In addition, we measured the effect of NaCl on the motility of UvrA-Qdot and UvrAB-Qdot complexes; we found that there was little increase in motility at low NaCl. Indeed we raised the concentration of NaCl to 1 M before we were able to observe UvrA-Qdot diffusion. At this concentration of NaCl we determined the combined diffusion constant for UvrA-Qdot and UvrAB-Qdot to be 0.25 ($\pm$0.12)$\mu m^2 s^{-1}$ (n=17). Since this value is greater than the maximum theoretical limit to diffusion along the groove of DNA ($2.1 \times 10^{-2} \mu m^2 s^{-1}$ – see below), this implies that these complexes no longer traverse the DNA groove but instead travel along the DNA as an non-contoured rod. Surprisingly, these molecules still do not travel at the diffusional limit ($17.5 \mu m^2 s^{-1}$ – see below), therefore an energy barrier exists. We calculate this barrier to be $4.2 \kappa_B T$; very similar to that observed in lower NaCl conditions when the molecule is expected to traverse the DNA groove. This suggests that the contacts made with DNA are unchanged.

3. ***Supplemental Calculations***

3.1 Shear force on DNA during tightrope construction.

A wealth of information from manipulation of individual DNA molecules have provided a framework for single-molecule studies involving stretching of DNA (Bouchiat et al., 1999; Bustamante et al., 1994; Chu, 1991; Cluzel et al., 1996; Punkkinen et al., 2005; Smith et al., 1992; Strick et al., 2000; Wenner et al., 2002). Furthermore, various manipulation techniques have been used to stretch DNA molecules and investigate the interactions between DNA and proteins (Allemand et al., 2003; van Mameren et al., 2008). It is well established that in low force range (< 10 pN), DNA behaves as an ideal polymer. Its elastic behavior reflects a reduction of its entropy upon stretching, and can be modeled as a worm-like chain. Between approximately 10 pN to 60 pN, DNA stretches elastically following Hooke's law. When DNA is stretched at forces in this range the bases remain paired and the helical form is maintained. To calculate the tension experienced by DNA during the formation of DNA tight-ropes in our experiments, we firstly used equations for two dimensional laminar flows (Prasuhn, 1980): $dp/dx = -12\eta V/B^2$

Where dp/dx is the pressure drop, η is the viscosity of water, V is the velocity of the flow (flow rate/cross section area), and B is the height of the flow cell (120 μm).

Based on this calculation, we were able to ascertain the flow-rate at 5 μm above the flowcell surface; this is the upper value for the flow rate where DNA is located. From comparison with a recent study (Graneli et al., 2006) we estimate the force to be below 10 pN. In addition we have directly measured the rate of fluid flow at 5 μm in our flowcells (Andrew Dunn, University of Vermont; personal communication) to be 900 $\mu m s^{-1}$. At this flow velocity the force on the DNA is still expected to be below 10 pN.

To mechanistically estimate the force on the DNA we created a 'ball on a string' model. DNA will collapse into a bundle of radius defined by Random Flight theory:

$$r = \sqrt{L.A}$$

where L = contour length, A = Kuhn length (2x persistence length)

This bundle of DNA experiences hydrodynamic drag in flow according to Stokes' law:

$$F = 6.\pi.\eta.v.r$$

where η = viscosity of water and v = fluid velocity

As the DNA extends the amount of DNA available to bundle reduces therefore less drag is experienced. The force required to extend the DNA is given by the worm-like chain (WLC) model:

$$F = \frac{\kappa_B T}{4} \cdot \left(\frac{1}{4\left(1 - x/L\right)^2} - \frac{1}{4} + \frac{x}{L} \right)$$

Figure S4 shows the opposing hydrodynamic and WLC forces experienced by DNA at different extensions. It is clear that as the DNA extends the hydrodynamic drag decreases and the force resisting extension increases. At the point of intersection of these two relationships the extension and retraction forces balance indicating that the tension on the DNA at a flow rate of 900 μms^{-1} is 5.4 pN.

Figure S4. The Balance of Forces on DNA in Flow

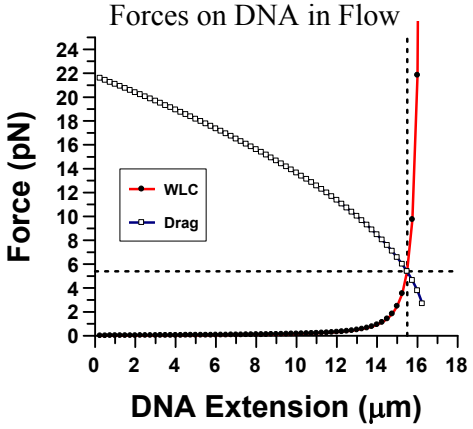

3.2 Inadequate searching based on a 3D distributive search alone

Firstly we assume that a typical *E.coli* cell has a division time of 20 minutes and that 200 molecules of UvrA are present, which is equivalent to 100 dimers. The footprint of UvrA is 33 bp (Van Houten et al., 1987) and we assume that recognition would occur anywhere within this region. We have shown here that the lifetime of interaction is 7 seconds, therefore 100 UvrA would search 3300 bp in 7 seconds, or 471 bp/s. In 20 minutes 5.7x10^5 bp would be searched. The *E.coli* genome of 4.6x10^6 bp, this is the equivalent of just 12% of the genome being searched in the time before division.

3.3 Statistical argument for UvrA hopping

Based on the data presented in this article the probability of detachment in one frame is given by:

Frame time/Attached lifetime = 0.483s/7s = 0.069

We calculated the number of time streaks in 512 frames of one dataset to be comprised of 87 non-hoppers & 60 hoppers = 147 time streaks

From this we calculate the interaction frequency:
Total time streaks/total number of frames = 147/512 = 0.29 events/frame

Therefore the combined probability that a molecule appears in the same frame from which one has also disappeared as:

Probability of detachmentxProbability of attachment = 0.069x0.29 = 0.02

Therefore the likelihood of such an event occurring is 1 in every 50 frames. The probability of every one of the 60 hoppers to have been due to the coincidental appearance and disappearance of UvrA-Qdot is unlikely: $0.02^{60} = 1.2\text{x}10^{-102}$.

3.4 Energy barriers to free diffusion

The expected diffusion constants were calculated from molecular radii based upon examination of the available structures of UvrA (Pakotiprapha et al., 2008), UvrB (Theis et al., 1999) and assuming a binding stoichiometry of $UvrA_2B$ (6.3 nm) and $UvrA_2B_2$ (7.2 nm). The radius of a quantum dot was based on the Stokes radius determined previously as 12.9 nm (Gorman et al., 2007), making the total UvrAB-Qdot complex radius ~13.5 nm. The barrierless diffusion constant for this complex moving along the DNA groove was calculated using the Stokes' law adapted to account for rotational energy losses (Schurr, 1979) resulting in a diffusion constant of $2.1\text{x}10^{-2}\ \mu m^2 s^{-1}$. Measured diffusion constants that exceeded this theoretical limit were no longer assumed to move along the DNA groove, and instead slide along DNA contour in a non-spiraling fashion. Molecules undergoing such motion no longer experience rotational friction and therefore the maximum calculated barrierless diffusion constant is approximately 800-fold higher at ~17.5 $\mu m^2 s^{-1}$.
Barriers to diffusion can be calculated by assuming the diffusion constant to occur as a series of steps of a single base pair in distance using the following relationship:

Steps.s^{-1} $(n) = 2D/(l_{bp})^2$ (Hughes, 1995)

Therefore the observed rate of stepping for a UvrAB-Qdot complex is:
$\triangleright\ 2\times(4.4\times10^{-4}\ \mu m^2 s^{-1})/(3.4\times10^{-4}\ \mu m)^2 = 7612 steps\cdot s^{-1}$

Barrierless diffusion results in a maximum stepping rate of:
$\triangleright\ 2\times(6.5\times10^{-3})\mu m^2 s^{-1}/(3.4\times10^{-4}\ \mu m)^2 = 363683 steps\cdot s^{-1}$

Applying the Arrhenius relationship it is possible to calculate the activation barriers to stepping for the observed and theoretical conditions respectively:
$k = e^{-E_A/\kappa_B T} \therefore E_A = -\ln(k)\cdot\kappa_B T$

$E_A = -\ln(7612)\cdot\kappa_B T = -8.9\kappa_B T$
$E_A = -\ln(363683)\cdot\kappa_B T = -12.8\kappa_B T$

The difference in energy yields the additional barrier that exists for the UvrAB-Qdot complex:

$$\Delta G_{E_A} = -8.9 - (-12.8)\kappa_B T = 3.9\kappa_B T$$

To calculate the diffusion constant of UvrAB in the absence of a Qdot we firstly removed the Stokes contribution of the Qdot from the complex. By calculating the new maximum rotational diffusion limit, as above, we could then calculate the effects of a $3.9\kappa_B T$ energy barrier on the diffusion constant of the UvrAB complex alone. This approach yields a diffusion constant for UvrAB of 3.5×10^{-3} $\mu m^2 s^{-1}$.

The distance scanned per encounter for a UvrAB complex can be calculated using (Hughes, 1995):

$$\triangleright \left(8n/\pi\right)^{1/2} = \sqrt{\frac{8}{\pi} \cdot 2Dt/l^2} = \sqrt{\frac{8}{\pi} \cdot \frac{2 \cdot (3.5 \times 10^{-3}\ \mu m^2 s^{-1}) \cdot 40s}{(3.4 \times 10^{-4}\ \mu m)^2}} = 2480bp$$

3.5 Positional accuracy

To assess the positional accuracy of our measurements we calculated the point spread function for a one-dimensional fit to our data. This method was used because accuracy was assessed from the sum of photons obtained from 10 randomly selected streaks (see streak analysis). The streaks chosen correspond to a Qdot bound to DNA and are projected in the plane parallel to the DNA filament. These therefore pertain to both the point spread function and the positional uncertainty due to Brownian motion of the DNA. A Gaussian was fit to the data for each streak and the background noise was assessed from the background adjacent to each peak. Using the equation below (Thompson et al., 2002) the mean accuracy was determined as 17.1(±2SEM) nm (equivalent to 50bp):

$$\sigma_i = \sqrt{\frac{s^2 + a^2/12}{N} + \frac{4s^3 b^2 \sqrt{\pi}}{aN^2}}$$

where s= standard deviation of the peak, a = pixel size (125 nm), b=standard deviation of the background, N=number of photons. Based on this analysis the barrier to higher resolution was background noise, which is expected given the experimental layout. In previous studies of Qdots attached to a surface, we have been able to attain higher levels of positional accuracy (6 nm – (Warshaw et al., 2005)). Therefore the Brownian motion of the Qdot on the DNA contributes to the elevated standard deviation of the peak, thus reducing the positional accuracy.

3.6 Monte Carlo simulations

To determine the effect of pauses on the appearance of the mean-squared displacement (MSD) plots, we performed a Monte Carlo based simulation. Using the calculated number of steps.s^{-1} for a one dimensional random walk with a diffusion constant of 2.5×10^{-2} $\mu m^2 s^{-1}$ as 432525 assuming each step is one base pair (see

above); we simulated 100 s of random walk resulting in 4.3×10^9 data points. To approximate the positional averaging expected from the integration times required for imaging, the average position after 1 second was used to determine the position of the random walker. One hundred individual runs were simulated, each with a new random number seed to represent 100 independent molecules. Using custom written software these were then compiled and averaged into MSD plots (Figure S5). To introduce pauses we re-used the random seeds and employed a probability filter, such that at random a pause in the data was introduced. The duration of the pauses were stochastically derived from an exponential distribution to represent a random process with a $t_{1/2}$ stated in the figure legends below. In addition we altered the number of pauses to determine the contribution of this factor to the MSD. Figure S6 shows the results from four simulations with increasing number of pauses. It is clear that in both cases pauses reduce the apparent diffusion constant rather than induce curvature in the MSD plot.

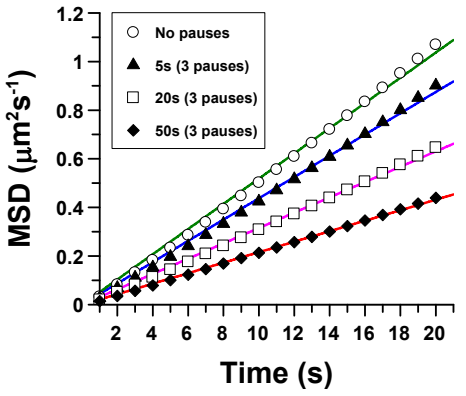

Figure S5. The Effect of Pause Duration on the Apparent MSD
In the absence of pauses a clear linear relationship between the MSD and time is seen as expected. The linear fit to these data produce a diffusion constant of $2.6(\pm 0.02SE) \times 10^{-2}$ $\mu m^2 s^{-1}$. We investigated three pause durations with $t_{1/2}$ of 5 s, 20 s and 50s the linear fits yield diffusion constants of $2.2(\pm 0.02SE) \times 10^{-2}$ $\mu m^2 s^{-1}$, $1.6(\pm 0.01SE) \times 10^{-2}$ $\mu m^2 s^{-1}$, $1.1\ (\pm 0.01SE) \times 10^{-2}$ $\mu m^2 s^{-1}$ respectively.

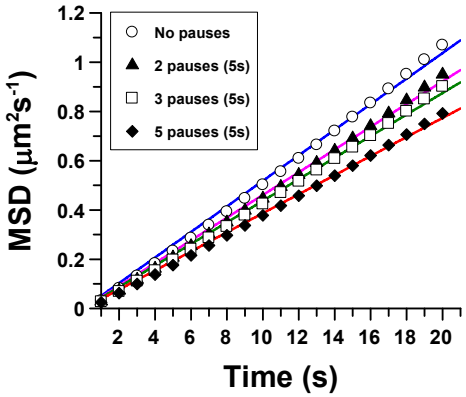

Figure S6. The Effect of Pause Frequency on the Apparent MSD
With two, three, and five pauses ($t_{1/2}$=5 s) a linear relationship is again seen with diffusion constants of $2.3(\pm 0.02SE) \times 10^{-2}$ $\mu m^2 s^{-1}$, $2.2(\pm 0.02SE) \times 10^{-2}$ $\mu m^2 s^{-1}$, $1.9\ (\pm 0.01SE) \times 10^{-2}$ $\mu m^2 s^{-1}$.

4. ***Supplemental References***

Allemand, J.F., Bensimon, D., and Croquette, V. (2003). Stretching DNA and RNA to probe their interactions with proteins. Curr Opin Struct Biol *13*, 266-274.

Bouchiat, C., Wang, M.D., Allemand, J., Strick, T., Block, S.M., and Croquette, V. (1999). Estimating the persistence length of a worm-like chain molecule from force-extension measurements. Biophys J *76*, 409-413.

Bustamante, C., Marko, J.F., Siggia, E.D., and Smith, S. (1994). Entropic elasticity of lambda-phage DNA. Science *265*, 1599-1600.

Chu, S. (1991). Laser Manipulation of Atoms and Particles. Science *253*, 861-866.

Cluzel, P., Lebrun, A., Heller, C., Lavery, R., Viovy, J.L., Chatenay, D., and Caron, F. (1996). DNA: an extensible molecule. Science *271*, 792-794.
Croteau, D.L., Dellavecchia, M.J., Wang, H., Bienstock, R.J., Melton, M.A., and Van Houten, B. (2006). The C-terminal zinc finger of UvrA does not bind DNA directly, but regulates damage-specific DNA binding. J Biol Chem *281*, 26370-26381.
Gorman, J., Chowdhury, A., Surtees, J.A., Shimada, J., Reichman, D.R., Alani, E., and Greene, E.C. (2007). Dynamic basis for one-dimensional DNA scanning by the mismatch repair complex Msh2-Msh6. Mol Cell *28*, 359-370.
Graneli, A., Yeykal, C.C., Prasad, T.K., and Greene, E.C. (2006). Organized arrays of individual DNA molecules tethered to supported lipid bilayers. Langmuir *22*, 292-299.
Hohng, S., and Ha, T. (2004). Near-complete suppression of quantum dot blinking in ambient conditions. J Am Chem Soc *126*, 1324-1325.
Hughes, B.D. (1995). Random Walks, Vol 1 (Oxford University Press).
Pakotiprapha, D., Inuzuka, Y., Bowman, B.R., Moolenaar, G.F., Goosen, N., Jeruzalmi, D., and Verdine, G.L. (2008). Crystal structure of Bacillus stearothermophilus UvrA provides insight into ATP-modulated dimerization, UvrB interaction, and DNA binding. Mol Cell *29*, 122-133.
Prasuhn, A.L. (1980). Fundamentals of Fluid Mechanics. 205-206.
Punkkinen, O., Hansen, P.L., Miao, L., and Vattulainen, I. (2005). DNA overstretching transition: ionic strength effects. Biophys J *89*, 967-978.
Ratcliff, G.C., and Erie, D.A. (2001). A novel single-molecule study to determine protein--protein association constants. J Am Chem Soc *123*, 5632-5635.
Sage, D., Neumann, F.R., Hediger, F., Gasser, S.M., and Unser, M. (2005). Automatic tracking of individual fluorescence particles: application to the study of chromosome dynamics. IEEE Trans Image Process *14*, 1372-1383.
Schurr, J.M. (1979). The one-dimensional diffusion coefficient of proteins absorbed on DNA. Hydrodynamic considerations. Biophys Chem *9*, 413-414.
Smith, S.B., Finzi, L., and Bustamante, C. (1992). Direct mechanical measurements of the elasticity of single DNA molecules by using magnetic beads. Science *258*, 1122-1126.
Strick, T., Allemand, J., Croquette, V., and Bensimon, D. (2000). Twisting and stretching single DNA molecules. Prog Biophys Mol Biol *74*, 115-140.
Tafvizi, A., Huang, F., Leith, J.S., Fersht, A.R., Mirny, L.A., and van Oijen, A.M. (2008). Tumor suppressor p53 slides on DNA with low friction and high stability. Biophys J *95*, L01-03.
Theis, K., Chen, P.J., Skorvaga, M., Van Houten, B., and Kisker, C. (1999). Crystal structure of UvrB, a DNA helicase adapted for nucleotide excision repair. EMBO J. *18*, 6899-6907.
Thompson, R.E., Larson, D.R., and Webb, W.W. (2002). Precise nanometer localization analysis for individual fluorescent probes. Biophys J *82*, 2775-2783.
Van Houten, B., Gamper, H., Sancar, A., and Hearst, J.E. (1987). DNase I footprint of ABC excinuclease. J Biol Chem *262*, 13180-13187.
van Mameren, J., Peterman, E.J., and Wuite, G.J. (2008). See me, feel me: methods to concurrently visualize and manipulate single DNA molecules and associated proteins. Nucleic Acids Res *36*, 4381-4389.
van Oijen, A.M., Blainey, P.C., Crampton, D.J., Richardson, C.C., Ellenberger, T., and Xie, X.S. (2003). Single-molecule kinetics of lambda exonuclease reveal base dependence and dynamic disorder. Science *301*, 1235-1238.

Wang, H., DellaVecchia, M.J., Skorvaga, M., Croteau, D.L., Erie, D.A., and Van Houten, B. (2006). UvrB domain 4, an autoinhibitory gate for regulation of DNA binding and ATPase activity. J Biol Chem *281*, 15227-15237.
Wang, H., Tessmer, I., Croteau, D.L., Erie, D.A., and Van Houten, B. (2008). Functional characterization and atomic force microscopy of a DNA repair protein conjugated to a quantum dot. Nano Lett *8*, 1631-1637.
Warshaw, D.M., Kennedy, G.G., Work, S.S., Krementsova, E.B., Beck, S., and Trybus, K.M. (2005). Differential labeling of myosin V heads with quantum dots allows direct visualization of hand-over-hand processivity. Biophys J *88*, L30-32.
Wenner, J.R., Williams, M.C., Rouzina, I., and Bloomfield, V.A. (2002). Salt dependence of the elasticity and overstretching transition of single DNA molecules. Biophys J *82*, 3160-3169.
Yang, H., Luo, G., Karnchanaphanurach, P., Louie, T.M., Rech, I., Cova, S., Xun, L., and Xie, X.S. (2003). Protein conformational dynamics probed by single-molecule electron transfer. Science *302*, 262-266.